Geophys. J. Int. (1995) **122**, 815–836

Coseismic crustal deformation from microseismicity in the Patras area, western Greece

Nikolaos S. Melis,[1]* Paul W. Burton[2] and Mike Brooks[1]

[1]*Department of Geology, University of Wales College of Cardiff, PO Box* 914, *Cardiff* CF1 3YE *UK*
[2]*School of Environmental Sciences, University of East Anglia, Norwich* NR4 7TJ *UK*

Accepted 1995 February 24. Received 1995 January 19; in original form 1994 July 28

SUMMARY

The Patras area lies in the western part of central Greece. It is an area characterized by high seismicity and complex neotectonics. Several devastating earthquakes have occurred in the region since 600 BC. Contemporary crustal deformation is examined in this area using microearthquake data recorded over a lengthy period, during 1983–84, by the Patras Seismic Network, principally, and to a lesser extent by the Volos Seismic Network.

The microseismicity (1.8–3.9 M_L) defines a zone deepening to the NE, which justifies a possible extension of the Gulf of Corinth major graben towards the Trikhonis Lake to the NW.

Spectra of 108 well-located microearthquakes are estimated, using *P*-waves obtained by selective windowing designed to include only the *P*-phase; seismic moments in the range $0.3–45.7 \times 10^{12}$ N m are obtained, accompanied by estimates of seismotectonic source parameters including source radii, average stress drop and average coseismic slip.

Poor correlation is found between seismic moment and magnitude, and the likely reason is the complex nature of the neotectonic regime existing in the area.

Two zones differing in crustal deformation characteristics are observed. The Corinth–Trikhonis zone reveals two sets of characteristic faults. The first set is represented by microearthquakes showing distinctive and relatively higher seismic moments in conjunction with lower stress drops and seismic slips. This set of faults shows greater source radius than the second set, and therefore the faults are longer. The second set is characterized by an almost constant source radius within the range of uncertainty, and a wide range of seismic moments, stress drops and seismic slips. The Rio zone is characterized by low seismic slip, stress drop and fault radii, with the exception of the locality south of the city of Patras, where relatively higher seismic slip, stress drop and fault radius are observed.

Key words: crustal deformation, Greece, microearthquakes, seismotectonics.

1 INTRODUCTION TO THE PATRAS AREA

In the present study, the Patras area is defined informally as an area including the Gulf of Patras and surrounding coastal areas, the adjacent part of the Gulf of Corinth and the area east of Trikhonis Lake (Fig. 1). As discussed by Brooks *et al.* (1988) and Melis, Brooks & Pearce (1989), the Patras area is a complex area in terms of seismotectonics. It lies at the junction of two different structural trends within a regional neotectonic regime involving approximately N–S extension (Fig. 1). The first is the WNW–ESE zone of extension defined by the Gulf of Corinth graben (Brooks & Ferentinos 1984), which possibly extends north-westwards to Trikhonis Lake (Melis 1986; Melis *et al.* 1989); the second is the NE–SW faulting associated with the Rio graben (Kontopoulos & Doutsos 1985), which has been interpreted as a transfer (transtensional) fault zone linking the Gulf of Patras graben in the south-west with the Corinth–Trikhonis zone of extension in the north-east (Melis 1986; Brooks *et al.* 1988; Melis *et al.* 1989; Fig. 1).

Several studies have been conducted on this graben system. Brooks & Ferentinos (1984) and Higgs (1988)

* Now at: 89[A] Asimakis Fotilas Str, GR-262 24 Patras, Greece.

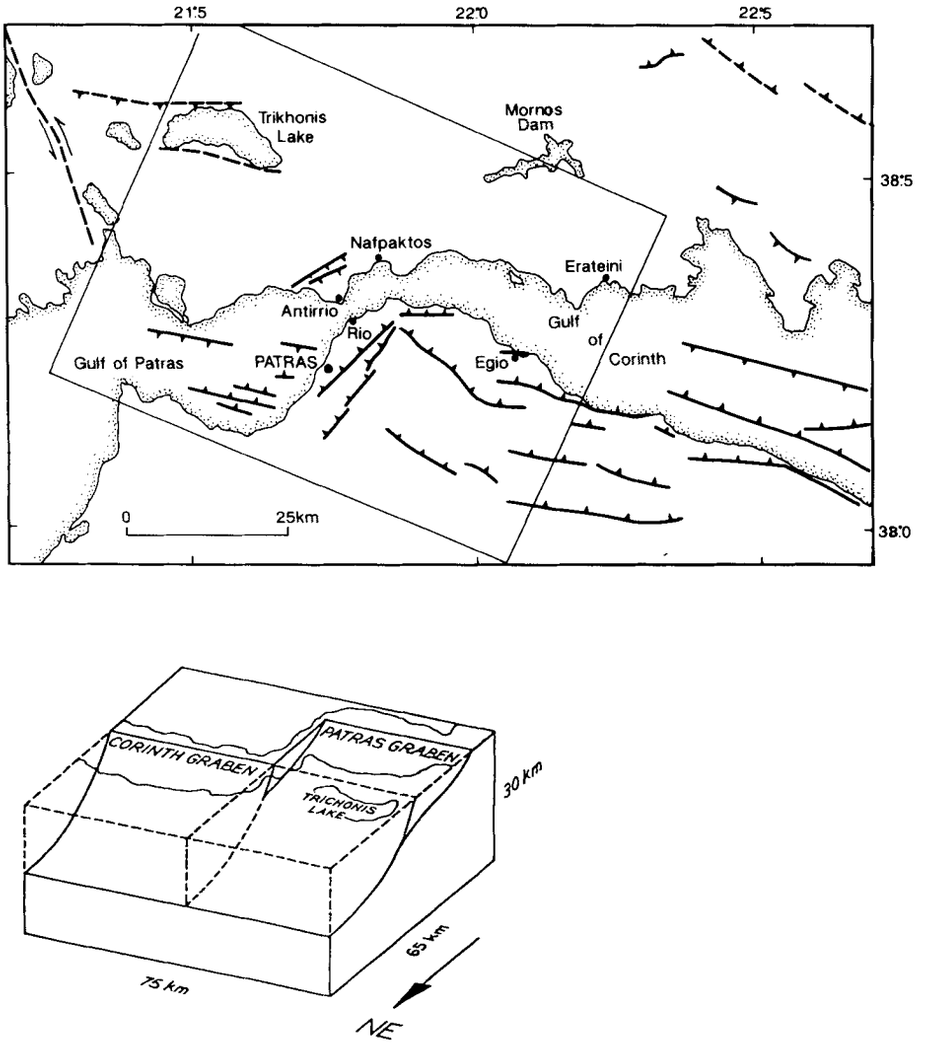

Figure 1. The neotectonic system of the Patras area and surrounding region, in western central Greece (after Ferentinos *et al.* 1985; Brooks *et al.* 1988; Melis *et al.* 1989). Footwall geometry of the extensional neotectonic system showing the Corinth–Trikhonis link transferred through the Rio transtensional zone to the Patras graben (after Melis 1986; Melis *et al.* 1989).

studied the structure of the Corinth graben offshore. They showed the WNW–ESE master fault that defines the graben to the south and the faults forming in the hanging wall. However, they did not have good-quality seismic profile data to extend their study to the western end of the Corinth graben. Onshore studies (e.g. Jackson *et al.* 1982; Vita-Finzi & King 1985; King *et al.* 1985; Doutsos & Piper 1990; Collier & Dart 1991) showed that the tectonic regime to the south and east of the Corinth graben is dominated by normal faulting of a WNW–ESE trend.

Ferentinos, Brooks & Doutsos (1985) studied the Patras graben offshore and showed that the seabed is affected by synsedimentary faulting with the same WNW–ESE trend. A follow-up study by Chronis, Piper & Anagnoston (1991) showed the same pattern of active faulting. Zelilidis, Koukouvelas & Doutsos (1987) described a tectonic regime with a similar WNW–ESE trend onshore, immediately east of the eastern end of the Patras graben. This coexists with a NE–SW fault regime defining the Rio graben, which was studied onshore by Kontopoulos & Doutsos (1985), mainly to the north in the Antirrio locality, and by Doutsos & Poulimenos (1992) in the Patras area and its surroundings. Offshore studies in the immediate vicinity show the existence of a complicated system of active faults with several trends, of which NE–SW and NW–SE appear to be the most dominant (Perisoratis, Mitropoulos & Aggelopoulos 1986; Chronis *et al.* 1987).

Following the study of Kontopoulos & Doutsos (1985), Doutsos, Kontopoulos & Frydas (1987), Doutsos, Kontopoulos & Poulimenos (1988) and Doutsos & Poulimenos (1992) suggested that the Rio graben developed earlier than the Corinth graben. Thus, as it is an extensional tectonic feature of the NE–SW trend, it could well develop right-lateral strike-slip motion if reactivated by the current regionally dominant N–S extensional regime forming the Corinth, Patras and Trikhonis grabens (Fig. 1). Brooks *et al.* (1988) and Melis *et al.* (1989), in their seismotectonic model for the region based on local microseismicity data (Melis

1986), suggested that Rio–Antirrio may behave as a transtensional fault zone linking the Corinth–Trikhonis graben system with the Patras graben (Fig. 1).

A preliminary microearthquake study of the area showed that its north-eastern segment in the Rio–Antirrio district exhibits very high seismic activity (Melis 1986; see also Section 2.2). Approximately 200 earthquakes of local magnitude less than 3.5 M_L occurred daily during 1983–1984. In terms of earthquake risk, it is important to recognise that Patras, the third largest city in Greece, lies only 8 km south-west of Rio (Fig. 1). In addition, a 3.5 km long bridge is being planned to span the Rio–Antirrio crossing. Finally, the Mornos Dam lies to the north of the study area. Hence, earthquake hazard investigations are of great importance to engineering projects in the Patras area, which is also of great interest in the study of local coseismic crustal deformation mechanisms.

2 SEISMICITY OF THE PATRAS AREA

2.1 Historical seismicity in the Patras area

Macroearthquake catalogues and earthquake studies of the Aegean region, and particularly of the area of central Greece (Galanopoulos 1960, 1961, 1981; Papazachos 1976; Makropoulos & Burton 1981; Papazachos & Comninakis 1982a,b; Comninakis & Papazachos 1986; Makropoulos, Drakopoulos & Latousakis 1989; Papazachos & Papazachos 1989; Ambraseys & Jackson 1990; Papazachos 1990) show a seismic gap in the Gulf of Patras (Fig. 2). However, large-magnitude events have occurred in the Narrows area and especially at locations near Nafpaktos, Erateini, Egio, Rio and Patras (Fig. 1). Some events have also occurred south-east of Trikhonis Lake, between the lake and Nafpaktos, thus justifying the suggested structural link between Trikhonis and the Gulf of Corinth (Melis 1986; Melis *et al.* 1989).

The historical data for the Patras area and surrounding region can be divided into two periods: pre-1900 and 1900–1986. Fig. 2 shows the distribution of events during these two periods. Locations for the first period are those listed in Table 1 [taken mainly from the most recently updated Papazachos & Papazachos (1989) historical catalogue], and for the second period are taken from the most recent instrumental catalogue (Makropoulos *et al.* 1989). However, some further corrections and entries have been made, which take into account all the information provided by the other historical catalogues mentioned above, and these are noted in the comments in Table 1.

The western end of the Gulf of Corinth exhibits the most activity. Damaging earthquakes have occurred in Helice (373 BC winter and 1861 December 26), south-east of Egio (Richter 1958), Egio, Erateini (1965 July 6; Ambraseys & Jackson 1990), Nafpaktos, Trikhonis and Patras (Papazachos

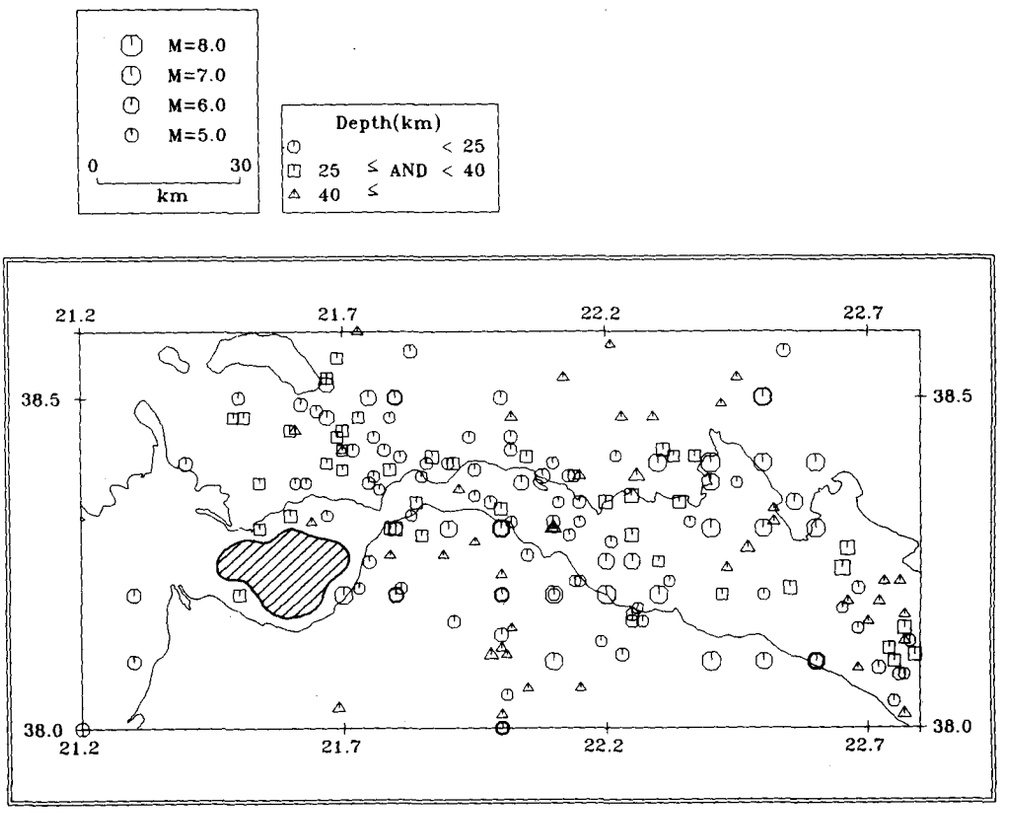

Figure 2. Epicentral map of earthquakes in western central Greece covering the whole period 600 BC to 1985 AD inclusive. Locations taken from the Makropoulos *et al.* (1989) catalogue and the list in Table 1. Note the gap (shaded) in seismicity in the Gulf of Patras and the link of seismicity between Corinth and Trikhonis.

Table 1. Historical seismicity in central Greece: pre–1900.

TIME (year)	date	hr	min	LAT (°N)	LON (°E)	DEPTH (km)	MAG (Ms)	COMMENTS (*)
	BC							
600				38.3	22.6	s	6.8	in (P&C 1982)/38.5/22.5 (G 1961)
373	WINTER	NIGHT		38.2	22.2	s	7.0	
348				38.4	22.5	s	6.7	
279				38.4	22.6	s	6.8	
	AD							
23				38.3	22.0	s	6.5	
551	JUL 7			38.4	22.4	s	7.2	
996				38.3	22.4	s	6.8	
1147				38.50	22.50	s	6.25	VIII-IX Galaxidi (Galan. 1981)
1402	JUNE			38.1	22.4	s	7.0	
1580				38.4	22.3	s	6.7	
1660	MAR			38.3	22.5	s	6.4	
1714	JUL 27	6	0	38.2	21.7	s	6.6	5.5 in Galanopoulos (1981)
1742	FEB 22			38.1	22.5	s	6.0	21 date corrected 22
1748	MAY 27	15	0	38.2	22.2	s	6.8	25 date corrected 27
1753	MAR 8			38.1	22.6	s	6.2	6 date corrected 8
1785	JAN 31	4	0	38.2	21.7	s	6.6	6.3 in Galanopoulos (1981)
1804	JUN 8	3	0	38.2	21.7	s	6.6	
1806	JAN 23			38.3	21.9	s	6.3	
1817	AUG 23	8	0	38.2	22.1	s	6.5	38.3/22.3/7.3 in Galan. (1981)
1861	DEC 26	6	30	38.2	22.3	s	6.7	7.5 in Galanopoulos (1981)
1862	JAN 1			38.25	22.25	s	6.0	Aftershock from Galan.(1981)
1870	AUG 1	0	41	38.5	22.5	s	6.8	7.3 in Galanopoulos (1981)
1876	AUG 6	11	0	38.25	21.75	s	4.70	VI Patra (Galanopoulos 1960)
1883	NOV 14	0	45	38.25	21.75	s	4.70	VI Patra (Galanopoulos 1960)
1885	FEB 18	14	30	38.50	21.75	s	5.8	from Galanopoulos (1981)
1885	JUL 14	0	4	38.25	21.75	s	4.70	VI Patra (Galanopoulos 1960)
1887	OCT 3	22	53	38.1	22.6	s	6.3	38.3/22.8 in Galan. (1981)
1888	SEP 9	15	15	38.1	22.1	s	6.2	6.0 in Galanopoulos (1981)
1889	AUG 25	19	13	38.3	20.1	61	7.0	hr/min from Galan. (1960)

s: shallow earthquakes (depth ≤ 60 km).

(*): all additional intensity/place data and corrections in the comments column taken from Galanopoulos (1960, 1961, 1981) and Papazachos & Comninakis (1982a). Corrections on dates are based on the knowledge that the old − new calendar difference is 13 days and not 11 days as is assumed in Papazachos & Papazachos (1989). Intensity to magnitude conversion is based on Makropoulos & Burton (1981).

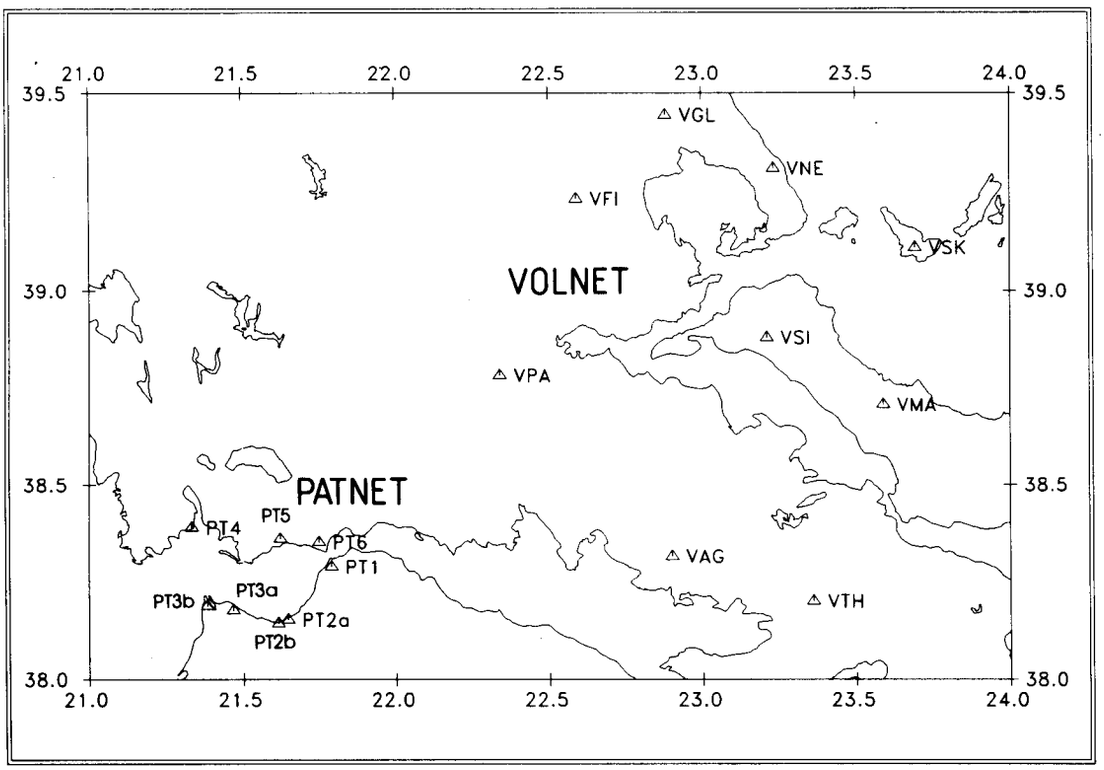

Figure 3. The VOLNET and PATNET station distribution.

& Papazachos 1989). Some of these earthquakes also triggered tsunami, for example Helice, Egio and Patras (Papazachos & Papazachos 1989). It is clear from the macroseismicity that the extensional zone of Corinth–Trikhonis, in particular the Rio–Antirrio district, and the area of the city of Patras are historically the most seismically active. However, large earthquakes are not documented in the immediately adjacent major tectonic feature of the Gulf of Patras.

A catalogue of focal mechanisms for earthquakes with surface-wave magnitude greater than 5.0 M_s for the area of central Greece is reported in Ambraseys & Jackson (1990). This coincides with all previous presentations for our study area (Papazachos 1976; Drakopoulos & Delibasis 1982; Papazachos *et al.* 1984; Papadopoulos *et al.* 1986) and also with the focal mechanisms presented in Melis *et al.* (1989). An approximately N–S extensional stress is dominant over the whole region.

2.2 Microseismicity in the Patras area

Two microearthquake networks have recently operated for lengthy periods in the area of central Greece, namely the VOLNET and PATNET networks (Fig. 3). Figs 4(a) and (b) illustrate the epicentres of the activity recorded by the two networks, respectively, for the Patras area. The Gulf of Patras seismic gap, the Narrows high seismic activity and the seismic link between Trikhonis Lake and the Gulf of Corinth are again all reflected in the microseismicity, as in the macroseismicity (Section 2.1).

108 well-located events (Table 2) were selected, using the following criteria:

(a) 5 km maximum error in computed locations of both epicentre and depth;

(b) a minimum number of five stations reporting clear *P*-wave recordings; and

(c) a maximum computed rms traveltime residual of 0.5 s.

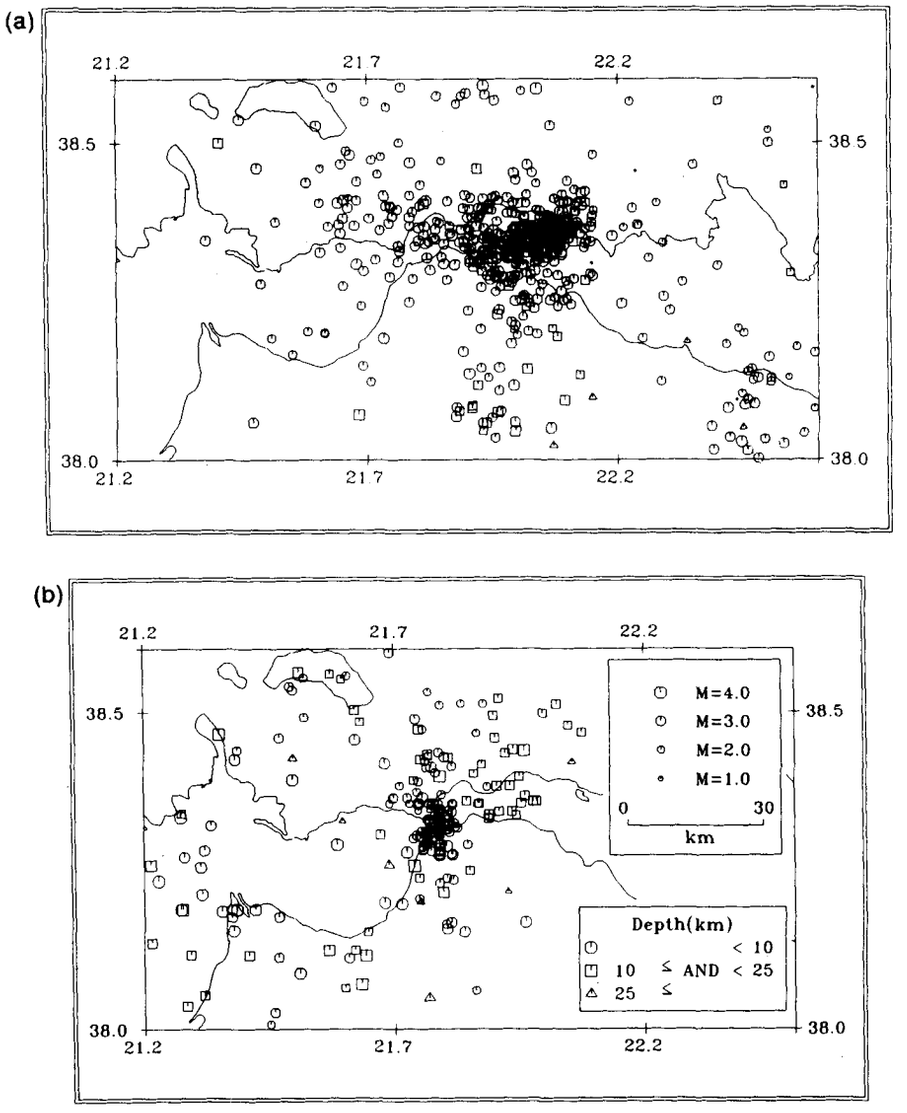

Figure 4. (a) Epicentral map of microearthquakes recorded by VOLNET during 1983–1984 in the Patras area and surrounding region. (b) Epicentral map of microearthquakes recorded by PATNET in the Patras area and surrounding region during 1983 July–1984 January. Events recorded by at least five stations.

Table 2. Hypocentral coordinates, magnitudes and location errors for the 108 selected PATNET and VOLNET events recorded in the Patras area. Event identifications are noted with V for VOLNET and P for PATNET. Magnitudes have been calculated in the normal way (Richter 1958). Otherwise, where N is indicated, only vertical components were used (as the only ones available), and a correction (+0.3) was applied (Burton *et al.* 1991) to convert these M_{LV} magnitudes to standard M_L local magnitudes. Where H is indicated, only one horizontal component was available and this was used. In this case a correction (+0.09) was suggested (Burton *et al.* 1991), but it was not used, being small and poorly resolved.

Event Id	Origin time (Y-M-D hr min sec)	Latitude (°N min)	Longitude (°E min)	Depth (km)	M_L	RMS (sec)	ERH (km)	ERZ (km)
1V	83 210 1957 8.13	38 24.39	22 7.07	6.04	2.5	0.37	3.8	3.8
2V	83 318 1331 41.36	38 21.21	21 55.94	1.00	2.3	0.29	4.5	4.3
3V	83 321 722 10.87	38 21.91	22 6.32	2.16	3.2	0.50	4.3	4.7
4V	83 619 514 22.45	38 22.92	21 42.25	0.98	2.9	0.50	4.6	3.2
1P	83 718 2224 52.42	38 30.72	22 1.51	20.24	2.8	0.06	2.1	1.7
2P	83 719 118 39.96	38 7.11	21 17.56	13.49	2.9	0.07	7.9	5.7
3P	83 719 359 55.24	38 33.46	21 36.41	6.36	2.3	0.02	1.0	2.0
4P	83 719 2357 55.06	38 2.19	21 17.04	20.19	3.1	0.03	4.4	2.7
5P	83 722 20 3 6.39	38 20.63	21 44.94	7.00	1.8	0.08	3.5	3.9
6P	83 723 1955 8.21	38 6.82	21 36.54	5.51	3.2	0.00	0.2	0.4
7P	83 724 616 46.74	38 19.59	21 47.42	3.25	2.6	0.14	1.5	1.7
8P	83 724 2124 56.52	38 20.43	21 47.41	7.00	2.4	0.04	2.9	2.6
5V	83 728 1614 14.16	38 23.36	21 59.79	1.22	2.8N	0.48	3.4	2.3
9P	83 8 5 658 4.01	38 12.08	21 45.12	27.15	2.5	0.00	0.2	0.5
10P	83 8 8 810 23.61	38 25.07	21 40.88	1.75	3.5	0.14	1.0	3.2
11P	83 8 8 2145 36.51	38 31.91	21 46.10	5.57	2.2	0.00	0.2	0.4
12P	83 810 15 0 37.68	38 29.85	21 59.84	16.71	2.5	0.00	0.5	0.2
13P	83 811 117 38.48	38 18.58	21 46.77	7.00	2.6	0.13	3.1	2.7
14P	83 811 230 50.97	38 20.20	21 56.61	20.42	2.4	0.03	3.3	2.5
15P	83 811 1430 20.38	38 25.92	21 45.98	10.33	3.0	0.11	3.0	2.8
16P	83 812 0 4 35.47	38 28.73	22 2.87	23.03	2.5	0.06	5.0	2.8
17P	83 812 1344 41.46	38 19.68	21 35.81	25.54	2.2	0.09	2.1	5.6
18P	83 813 840 26.77	38 18.38	21 40.37	16.81	2.8	0.01	0.2	0.4
19P	83 814 10 4 10.64	38 33.14	21 35.78	18.30	2.2	0.07	4.8	4.7
20P	83 814 1641 0.52	38 20.24	21 53.35	13.64	3.1	0.11	2.5	1.2
21P	83 816 1821 32.18	38 25.46	21 45.14	11.76	2.8	0.02	0.7	0.8
6V	83 816 2251 24.43	38 18.93	22 2.39	0.68	2.8	0.49	3.3	3.1
7V	83 824 2111 46.94	38 23.07	22 5.65	3.93	3.3	0.43	3.7	4.1
22P	83 914 1427 24.83	38 25.67	21 48.41	16.19	2.7	0.01	0.5	0.4
23P	83 914 2221 31.00	38 18.41	21 45.69	5.84	2.6	0.06	3.7	6.1
24P	83 916 1736 58.12	38 20.74	21 47.42	3.70	2.6	0.04	2.9	3.8
25P	83 917 855 8.54	38 21.82	21 41.99	7.50	2.6	0.09	2.7	3.6
26P	83 920 1310 8.28	38 7.54	21 34.14	12.61	3.5	0.08	4.3	5.3
8V	8310 6 233 4.28	38 12.39	22 4.10	24.48	2.2	0.16	3.8	3.6
9V	8310 7 1919 38.20	38 12.31	21 59.56	24.00	2.2N	0.09	2.8	2.3
10V	8311 3 252 36.73	38 23.73	21 56.91	0.66	2.8N	0.30	3.3	2.5
27P	831119 023 22.28	38 25.28	21 45.68	3.55	2.3	0.10	4.3	4.7
28P	831119 5 8 57.18	38 14.32	21 45.02	19.28	2.5	0.01	0.9	1.7
29P	831119 1725 40.86	38 27.97	21 51.77	9.91	2.3	0.12	3.9	5.3
30P	831120 649 3.26	38 29.65	21 53.83	11.38	2.7	0.02	2.8	1.7
31P	831120 2227 21.59	38 33.78	21 30.63	16.94	3.3	0.11	2.9	4.3
32P	831120 2347 31.79	38 33.24	21 31.26	9.86	2.4	0.03	2.0	3.0
33P	831125 1442 1.44	38 25.69	21 47.95	6.35	3.1	0.06	3.3	2.4
34P	831126 1027 50.49	37 55.37	21 34.70	36.30	3.9	0.02	3.9	4.5
35P	831127 536 37.86	38 21.54	21 50.61	10.75	2.6	0.14	4.3	2.4
36P	831129 236 4.20	38 31.29	21 54.49	11.57	2.6	0.02	2.5	1.5
37P	8312 5 149 29.37	38 30.80	21 50.00	9.82	2.2	0.01	1.7	1.1
38P	8312 6 2 9 18.48	38 25.74	21 46.06	17.20	2.2	0.01	0.5	0.4
39P	831212 1230 51.94	38 7.07	21 24.49	12.22	3.1	0.02	2.1	1.7
40P	831213 748 33.05	38 23.48	21 44.35	15.43	2.4	0.03	1.4	1.2
41P	831213 851 3.35	38 24.99	21 52.44	19.22	2.3	0.03	3.3	2.4
42P	831214 553 22.81	38 26.02	21 55.24	17.22	2.7	0.07	0.7	0.4
43P	831224 2045 29.79	38 27.52	21 54.01	10.88	2.8	0.03	3.2	1.8
44P	831225 23 7 27.79	38 26.40	21 56.16	19.27	3.2	0.06	6.3	3.8
45P	831225 2314 52.15	38 18.81	21 47.62	7.00	2.9	0.04	3.2	3.5
46P	831226 2 9 7.81	38 25.45	21 22.85	4.44	2.1	0.11	2.9	4.7
47P	831228 351 12.28	38 32.09	21 29.94	9.20	2.8	0.05	3.2	4.6
48P	831228 1724 14.07	38 29.07	21 37.92	14.06	2.4	0.07	3.9	3.1
49P	831229 630 23.51	38 18.13	21 45.11	5.09	2.5	0.13	0.7	1.4
50P	831231 233 9.23	38 22.36	21 44.77	9.94	2.3	0.12	1.6	1.4
51P	831231 1430 28.49	38 22.96	21 55.85	17.74	2.9	0.10	3.4	1.6
52P	831231 1628 31.51	38 21.28	21 44.94	7.00	2.1	0.13	4.7	4.7
53P	84 1 1 310 10.22	38 24.78	21 48.84	9.72	2.5	0.10	3.1	2.5
54P	84 1 1 357 11.01	38 21.48	21 58.65	21.82	2.8	0.11	3.8	1.8
55P	84 1 2 911 35.14	38 21.35	21 57.23	17.61	2.9	0.05	10.6	6.6
56P	84 1 2 926 27.10	38 18.48	21 47.42	7.00	2.8	0.07	2.9	3.3
57P	84 1 2 1220 35.03	38 20.53	21 54.54	19.37	2.7	0.11	3.6	1.8
58P	84 1 2 14 8 37.98	38 18.98	21 49.52	4.53	2.6	0.08	4.9	3.2
59P	84 1 2 2049 2.36	38 21.52	21 59.06	22.21	2.8	0.11	4.3	2.0
60P	84 1 3 039 9.08	38 20.81	21 46.34	13.95	2.0	0.08	3.8	4.4
11V	84 1 3 250 48.87	38 18.61	21 51.20	1.02	3.3	0.48	4.9	3.8
61P	84 1 3 622 52.91	38 22.01	21 57.66	20.52	2.9	0.04	2.8	1.8
12V	84 1 3 1017 45.49	38 20.95	21 55.87	1.95	3.0N	0.49	3.3	2.8

Table 2. (*Continued.*)

Event Id	Origin time (Y-M-D hr min sec)	Latitude (°N min)	Longitude (°E min)	Depth (km)	M_L	RMS (sec)	ERH (km)	ERZ (km)
62P	84 1 3 1130 42.08	38 25.21	22 3.30	26.01	2.6	0.04	13.5	8.4
63P	84 1 3 1545 7.24	38 18.64	21 46.05	2.73	3.1	0.11	2.8	5.9
64P	84 1 3 1755 19.12	38 20.57	21 56.09	20.47	2.8	0.11	3.4	1.5
65P	84 1 3 2116 35.85	38 19.90	21 53.21	16.22	2.8	0.11	3.6	1.7
13V	84 1 5 1510 0.55	38 20.20	21 53.56	0.76	2.9N	0.46	4.6	3.6
66P	84 1 6 312 15.41	38 18.95	21 47.42	6.35	2.8	0.04	3.4	3.7
67P	84 1 6 1648 25.31	38 30.78	21 52.62	7.60	2.4	0.03	3.0	2.7
68P	84 1 6 2120 20.24	38 24.67	21 45.85	3.83	2.3	0.12	4.8	4.4
69P	84 112 1636 31.72	38 23.85	21 57.00	18.10	2.8	0.11	4.2	2.2
70P	84 116 147 52.87	38 28.35	21 45.39	8.74	2.4	0.01	0.8	0.7
14V	84 2 7 1929 32.87	38 21.79	21 57.09	0.97	3.4	0.43	5.0	4.8
15V	84 211 1110 7.53	38 21.82	21 53.24	0.52	3.0	0.45	4.8	4.1
16V	84 218 4 2 16.59	38 20.64	22 1.53	0.86	3.0N	0.45	3.6	3.4
17V	84 220 1548 17.66	38 20.97	22 0.23	0.87	3.0	0.40	4.7	4.4
18V	84 227 2121 28.25	38 19.96	21 59.80	1.45	2.8N	0.49	3.6	2.9
19V	84 324 2219 48.12	38 13.02	21 59.23	1.51	3.0	0.45	4.1	2.8
20V	84 423 1052 14.21	38 23.15	22 0.78	2.36	2.6	0.36	4.2	3.6
21V	84 5 1 1148 22.98	38 23.57	22 6.97	2.38	2.9N	0.44	3.8	4.3
22V	84 8 2 714 20.82	38 20.49	22 1.51	12.41	2.7	0.41	4.7	2.2
23V	84 8 9 246 14.01	38 22.69	22 6.16	4.32	2.5	0.32	3.8	4.5
24V	84 815 2051 4.97	38 21.36	22 2.40	1.19	2.9	0.42	3.1	4.0
25V	84 818 326 39.17	38 19.92	22 2.14	10.99	2.4	0.19	2.0	1.1
26V	84 819 1446 0.92	38 21.41	22 0.77	0.91	3.0	0.37	4.9	4.5
27V	84 9 1 1126 43.11	38 15.96	22 5.23	1.20	3.2	0.44	4.3	4.4
28V	84 929 3 1 27.87	38 18.81	22 4.34	0.07	2.9	0.26	4.2	4.1
29V	8411 9 1658 48.62	38 17.38	21 59.14	0.34	3.2N	0.34	3.5	2.0
30V	8411 9 2030 19.56	38 20.68	21 59.58	0.96	2.8	0.48	3.9	3.6
31V	841110 456 0.67	38 19.28	21 57.38	0.98	3.3N	0.48	4.2	3.3
32V	841112 922 51.91	38 20.16	21 59.99	0.89	3.3H	0.12	2.5	2.2
33V	841113 1229 5.13	38 17.83	21 57.34	7.55	2.7	0.47	4.5	3.5
34V	841115 1937 42.44	38 21.73	22 5.20	12.18	2.6	0.20	2.3	1.2
35V	841120 1930 25.40	38 23.00	22 2.63	1.58	3.0N	0.50	4.2	4.7
36V	841123 055 35.64	38 20.56	22 8.03	2.25	2.9	0.38	4.2	4.2
37V	841124 915 1.11	38 19.48	22 5.17	0.47	3.4	0.47	4.7	4.1
38V	841217 1 3 30.34	38 22.07	22 6.63	2.07	3.0	0.34	2.5	4.0

The spatial distribution of the well-located events (Fig. 5a) affirms the same features as the overall seismicity recorded by the two networks. An approximately SW–NE cross-section through Rio–Antirrio is produced using these well-located events (Fig. 5b), and adjacent crustal slices of 20 km width are also presented [Figs 5c(i) and (ii)] to show along-strike variations in the microseismicity pattern. The first slice [Fig. 5c(i)] is comparable to that presented by Melis *et al.* (1989), but utilizes VOLNET data in addition to PATNET data and shows a relative increase of activity in the hanging wall. The second slice [Fig. 5c(ii)], situated further to the west, shows a major increase of activity in the hanging wall. The Gulf of Patras gap and the Corinth master fault north-west of the Gulf of Corinth can be identified easily in both the individual slices and the main cross-section. The latter feature through the Narrows demonstrates seismically the Corinth–Trikhonis structural link. The main volume of seismic activity is in the hanging wall of the Corinth–Trikhonis half graben system with a relatively passive footwall.

The results from a temporary network covering the Peloponnesos for six weeks in 1986 show a similar spatial distribution of microseismicity in central Greece and produce a cross-section similar to Fig. 5(b) (Pedotti 1988; Hatzfeld *et al.* 1989, 1990). Once again, a zone of seismicity dipping towards the north-east with some activity in the hanging wall indicates the Corinth master fault extending north-west from the Gulf of Corinth and establishes a link with the Trikhonis graben.

Focal mechanisms for some 31 events were also produced [Table 3, Fig. 6, after Pedotti (1988) and Hatzfeld *et al.* (1989, 1990)], and these provide further support for the seismotectonic model of Melis *et al.* (1989). In particular, some dextral strike-slip focal mechanisms (20, 7: Fig. 6) coexist with a normal focal mechanism (21: Fig. 6) in the south-eastern part of the Gulf of Patras, and one dextral strike-slip focal mechanism (16: Fig. 6) also coexists with normal focal mechanisms in the north-eastern part of the Gulf of Patras (15, 17, 5 of approximately NW–SE, NE–SW and E–W strike, respectively: Fig. 6). There are also two compressional focal mechanisms in the south-eastern location (4, 6: Fig. 6). Focal mechanisms 28, 26 and 2 (Fig. 6) show WSW–ENE extension coexisting with NE–SW dextral strike slip at the extreme north-eastern point where the Rio–Antirrio transtensional zone meets and coexists with the Corinth–Trikhonis zone. As for the Corinth–Trikhonis link, focal mechanisms are not available north-west of Rio–Antirrio. Only some less reliable focal mechanisms (Hatzfeld, personal communication), marked with '+' signs, are available at the north-eastern end of Trikhonis Lake, and these show some dextral strike slip on E–W planes (11, 10: Fig. 6), coexisting with compressional NE–SW strike focal mechanisms. These less reliable determinations have not been taken into account in the present investigation.

3 SPECTRAL ANALYSIS OF WELL-LOCATED EVENTS IN THE PATRAS AREA

To extend investigation of the variation of coseismic deformation throughout the study area, seismotectonic

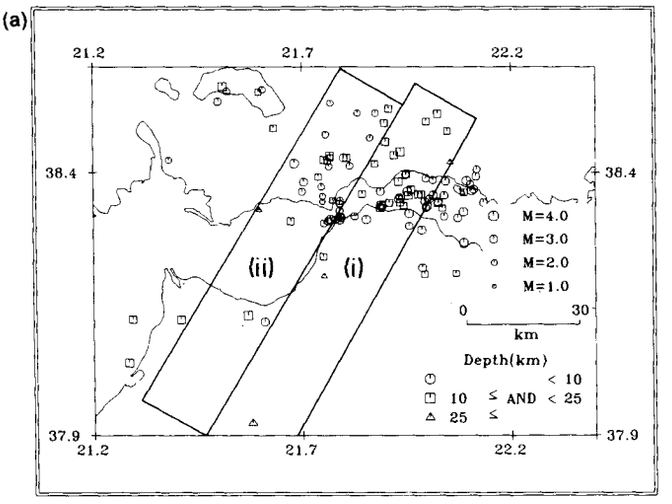

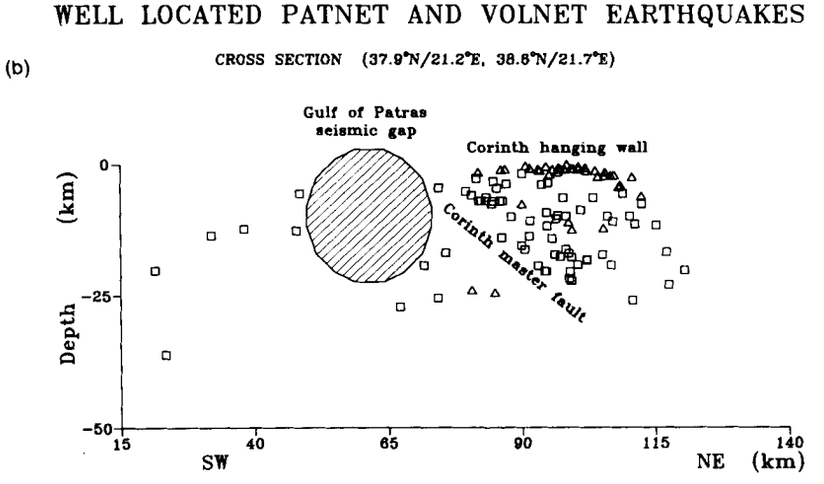

Figure 5. (a) Epicentral map of the 108 PATNET and VOLNET events selected for spectral analysis. Note the seismic gap in the Gulf of Patras, and the Corinth–Trikhonis seismic link. Boxes (i) and (ii) indicate the data used to produce the two SW–NE slices of 20 km width. (b) SW–NE cross-section using all data illustrated in (a), showing the Gulf of Patras seismic gap and the Corinth–Trikhonis dipping zone and exhibiting high seismicity in the hanging wall. (c) Slices (i) and (ii) of 20 km width located in (a).

source parameters of the microearthquakes are examined. There are many examples of the extraction of such parameters from spectra, including the previous studies of Keilis-Borok (1959), Trifunac (1972), Hanks & Wyss (1972), Thatcher & Hanks (1973), Archuleta *et al.* (1982), Modiano & Hatzfeld (1982), Gagnepain-Beyneix (1985), Brune *et al.* (1986), Burton & Marrow (1989) and Burton, Melis & Brooks (1995). All of these studies involve spectral analysis of *P*-wave data or *S*-wave data or both. *P*-wave spectral analysis is applied here to the 108 well-located events. The earthquake source parameters derived are seismic moment (M_0), stress drop ($\Delta\sigma$), source or 'fault' radius (r) and average coseismic slip (s).

The procedure involves a standard Fourier spectral analysis of a selected time window in the seismogram (in our case the *P*-window). A *P*-wave log–displacement spectrum is characterized by a model that has two essential components: a flat section with amplitude level Ω_0 up to a frequency f_c and a roll-off linear decay from f_c to an f_{max}. The long-period spectral level and the corner frequency are defined by two intersecting lines, fitted by eye to the overall mean trend of the low-frequency spectral asymptote and the high-frequency roll-off. These parameters determine the source characteristics of each event analysed. In practice, the two most important considerations are those of window selection and attenuation.

The spectral analysis procedure is described in detail elsewhere (Melis 1992; Burton *et al.* 1995), and was applied similarly here to the 108 well-located microearthquakes of Fig. 5(a) (listed in Table 2); it will only be described briefly. Two examples are shown in Fig. 7, taken from the earthquake of 1983 January 6 of magnitude 2.8 M_L (entry 66P in Table 2). The seismograms illustrated display clear *P*-wave arrivals, and for this earthquake clear *P*-wave recordings were obtained from five stations and the event is consistent with the criteria stated in Section 2.2. The first

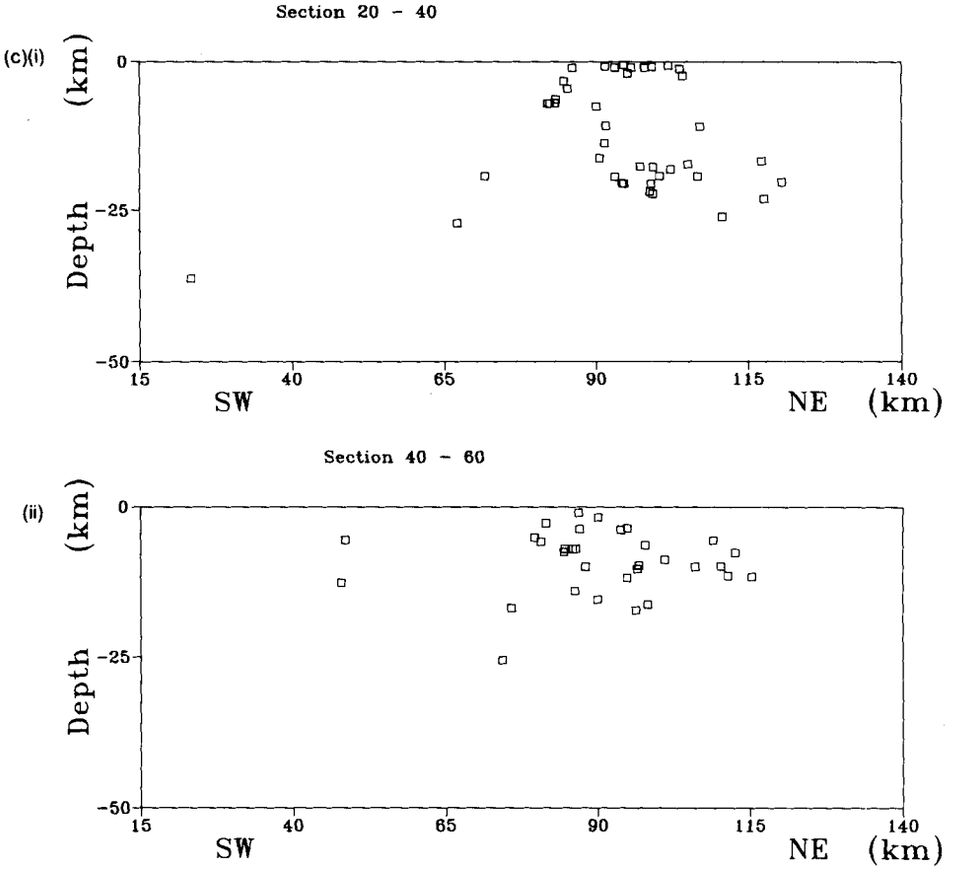

Figure 5. (*Continued.*)

Table 3. Focal mechanisms after Pedotti (1988) and Hatzfeld *et al.* (1989, 1990).

No	Time y/m/d	h/min sec.	Latitude °N-min	Longitude °E-min	Depth km	Mag ML	Plane 1 strike/dip	Plane 2 strike/dip	P-axis plunge/pl.dir	T-axis plunge/pl.dir.
1	860610	1315 39.33	38-10.34	21-25.38	7.15	1.78	280.0 50.0	40.0 59.2	54.7 255.7	5.3 158.1
2	860612	0447 41.07	38-22.32	21-56.67	11.59	1.86	100.0 70.0	260.0 21.2	64.3 21.6	24.7 184.5
3	860613	1521 29.10	38- 1.18	21-33.89	19.65	1.49	270.0 50.0	90.0 40.0	85.0 180.0	5.0 0.0
4	860613	1523 35.18	38- 1.01	21-34.09	19.63	2.66	310.0 40.0	160.0 54.0	7.2 236.8	73.2 121.9
5	860615	1921 58.71	38-21.89	21-47.64	5.10	2.59	270.0 30.0	90.0 60.0	75.0 0.0	15.0 180.0
6	860617	0252 26.00	38- 8.05	21-39.91	22.58	1.87	190.0 50.0	20.0 40.4	4.8 284.6	83.1 58.5
7	860617	0304 17.54	38- 8.03	21-39.11	23.13	1.96	230.0 90.0	140.0 90.0	0.0 95.0	0.0 5.0
8	860621	0212 35.79	38-19.23	22- 4.19	11.55	2.21	280.0 60.0	170.0 59.4	45.6 135.3	0.4 44.9
9	860621	0652 6.47	38-19.57	22- 3.56	11.88	2.53	310.0 60.0	60.0 59.4	45.6 274.7	0.4 5.1
10+	860622	0800 42.46	38-34.27	21-42.66	12.53	4.07	262.0 75.0	170.0 82.6	15.9 125.2	5.3 216.7
11+	860622	0921 28.23	38-33.39	21-40.56	16.44	3.65	270.0 80.0	170.0 45.4	38.2 140.8	21.9 32.3
12+	860622	1055 59.02	38-32.97	21-40.63	9.22	3.06	250.0 40.0	55.0 51.0	5.5 151.8	80.7 278.2
13	860623	1431 17.48	38-36.35	21-41.21	14.36	3.14	240.0 48.0	35.0 44.8	1.6 317.8	77.1 220.7
14	860623	2123 9.08	38- 3.36	21-36.36	16.18	2.60	40.0 30.0	310.0 90.0	37.8 246.6	37.8 13.4
15	860623	2155 55.44	38-19.38	21-40.85	36.59	2.27	220.0 70.0	330.0 46.8	46.6 174.8	14.0 280.1
16	860624	2204 31.03	38-20.80	21-46.25	17.64	4.14	290.0 80.0	20.0 90.0	7.1 245.4	7.1 154.6
17	860624	2212 9.24	38-21.19	21-47.08	10.66	2.85	210.0 60.0	0.0 33.7	70.4 155.7	13.6 288.4
18	860626	0256 31.45	38-14.45	21-54.89	16.11	2.82	180.0 70.0	310.0 29.5	59.0 121.2	21.9 253.3
19	860627	0530 20.42	38-19.74	22- 4.14	10.21	2.83	0.0 60.0	240.0 49.1	54.7 216.7	6.3 117.8
20	860628	2348 59.57	38- 8.15	21-38.33	19.83	3.43	225.0 90.0	315.0 90.0	0.0 270.0	0.0 180.0
21	860628	2352 55.72	38- 9.52	21-38.78	18.16	3.60	60.0 50.0	300.0 59.2	54.7 264.3	5.3 1.9
22-	860702	1721 10.51	38- 8.47	22- 1.93	53.67	1.66	50.0 70.0	310.0 64.5	33.1 271.4	3.6 179.0
23	860704	1406 15.11	38- 7.62	21-58.49	25.93	3.48	280.0 60.0	20.0 73.3	33.9 243.4	8.6 147.6
24	860707	1714 55.68	38-16.34	21-46.45	6.65	2.36	240.0 90.0	180.0 0.0	45.0 150.0	45.0 330.0
25	860710	0357 53.50	38-20.38	21-59.92	8.37	2.80	220.0 40.0	80.0 57.3	67.5 39.8	9.2 152.8
26	860710	1814 28.44	38-25.69	21-56.40	21.26	2.88	130.0 60.0	38.0 86.5	18.1 87.9	23.3 349.8
27-	860713	0841 35.73	38- 4.31	22-36.65	69.43	1.91	60.0 60.0	310.0 59.4	45.6 275.3	0.4 184.9
28	860713	2122 47.33	38-25.04	21-47.35	18.55	2.53	210.0 70.0	110.0 64.5	33.1 71.4	3.6 339.0
29	860714	1715 8.43	38- 4.60	22- 2.66	13.16	3.17	210.0 40.0	30.0 50.0	85.0 300.0	5.0 120.0
30	860714	2254 59.48	38- 4.99	22- 3.51	13.43	1.78	30.0 70.0	130.0 64.5	33.1 348.6	3.6 81.0
31	860715	1112 25.82	38-19.66	22-11.78	16.06	2.87	210.0 70.0	310.0 64.5	3.6 261.0	33.1 168.6

'+': less reliably determined mechanisms.
'−': intermediate-depth earthquakes.

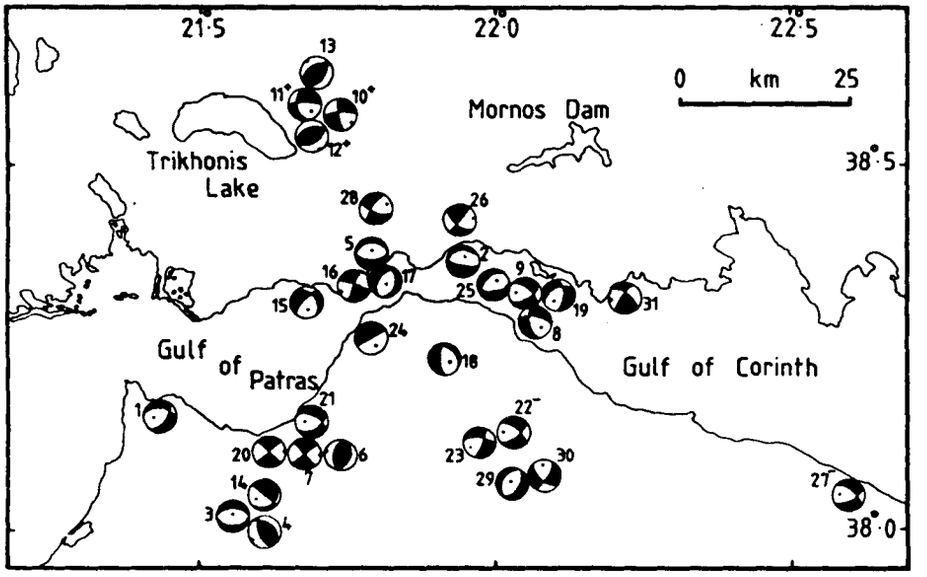

Figure 6. Focal mechanisms in central Greece for 31 microearthquakes recorded by the Peloponnesos network (after Pedotti 1988; Hatzfeld *et al.* 1989, 1990). Lower hemisphere equal-area projection; identification numbers are consistent with data in Table 3; '+' denotes a less reliably determined mechanism and '−' denotes the mechanism of an intermediate-depth earthquake.

example (Fig. 7a) is recorded at a short hypocentral distance of 7.0 km at station PT1 (Patras University), and the second example at a larger hypocentral distance of 38.9 km at station PT3b (Araxos). The short-range recording shows evidence of high-frequency content both in the seismogram and in the displacement spectrum relative to the longer range recording [the evidence in the displacement spectrum being the constant linear roll-off to higher frequencies in Fig. 7(a) than in Fig. 7(b); in Fig. 7(b) the Q correction distorts the spectrum at the highest frequencies at which it begins to amplify non-propagating energy when the signal-to-noise ratio is too low]. The fitting of the long-period asymptote and roll-off by eye is straightforward and indicates an f_c around 10 Hz. More than 1 000 displacement spectra were examined in this way. The correction for attenuation did not affect the values of Ω_0 and f_c for microearthquakes recorded by PATNET, whereas it made a small difference for those recorded by VOLNET that are recorded typically at a greater range. The family of Ω_0 and f_c values obtained from all the spectra are illustrated in Fig. 8, with $R\Omega_0$ values compensating for the hypocentral distance R km. When considering measurement uncertainties on f_c (or Ω_0) it is important to recognize that these observables are log-normally distributed, as the measurements are obtained from logarithmic displacement spectra. Two examples illustrate the actual measurement uncertainties on f_c; these are the earthquakes of 1983 July 18 with 2.8 M_L, and 1983 July 19 with 2.9 M_L (Table 2). The former was well recorded at six stations and generated six values of f_c, and the latter at five stations with four values of f_c ensuing. The mean values of log f_c, with one standard deviation range, are, respectively, $\log f_c = 1.013 \pm 0.08$ and 1.12 ± 0.07, corresponding to $f_c = 10.30^{+2.09}_{-1.73}$ Hz and $f_c = 13.18^{+2.31}_{-1.96}$ Hz, where the mean f_c value is not centrally placed in the ± one standard deviation range. In practice, standard deviation errors on Ω_0 and f_c are not calculated; instead ranges on the resulting values of seismic moment, source radius, average stress drop and coseismic slip described below are computed, bearing in mind that these computed quantities are also inherently log-normally distributed because of the original observational measurements.

Following the model of Brune (1970, 1971), the low-frequency spectral level Ω_0 is assumed to be proportional to the seismic moment M_0, and given by (Keilis-Borok 1959)

$$M_0 = 4\pi R\rho\alpha^3\Omega_0/kR_{\theta\Phi} \qquad \text{(in N m)}, \tag{1}$$

where ρ is the density of the medium (2700 kg m^{-3}), R is the hypocentral distance between source and receiver, α is the P-wave velocity at the source taken from the velocity model used to locate the events (Melis 1986, 1992), and the product $kR_{\theta\Phi}$ is a constant (commonly taken as 0.85) allowing for free surface reflection and the average radiation pattern. Modiano & Hatzfeld (1982) found Madariaga's (1976) dynamic model to be more realistic then Brune's and it is used here for calculation of source radius r. This is proportional to the corner frequency, f_c, for a circular model of fault rupture, and, for a rupture velocity of 0.9β (Madariaga 1976),

$$r = 0.32\beta/f_c \qquad \text{(in m)}, \tag{2}$$

where β is the S-wave velocity at the source (β is taken as $\alpha/1.78$ after King *et al.* 1985) and f_c is measured from a P-wave spectrum. Assuming the case of complete stress drop for a circular fault, the average stress drop ($\Delta\sigma$) is obtained from

$$\Delta\sigma = 7M_0/16r^3 \qquad \text{(in bar)} \tag{3}$$

(Keilis-Borok 1959; Kanamori & Anderson 1975), where M_0 and r are the values obtained previously. Slip s, averaged

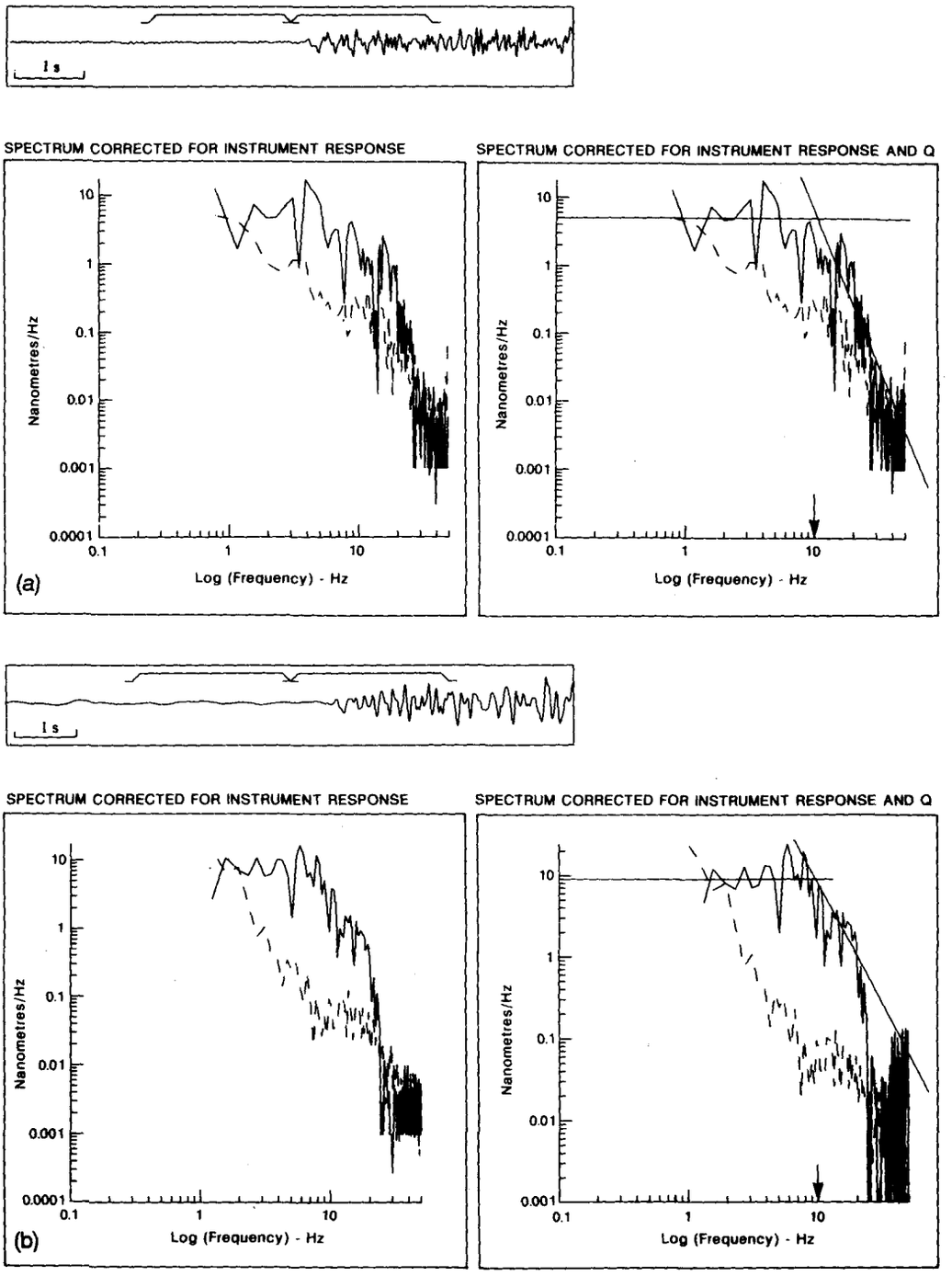

Figure 7. Examples of spectral analysis, illustrating the seismogram and selected *P*-wave window, preceding noise window, and logarithmic displacement spectrum of the *P*-wave corrected for the seismometer response (and noise spectrum shown as dashed line) and also for anelastic attenuation along the propagation path (Q). The long-period asymptote (Ω_0) to the spectrum and the high-frequency roll-off are fitted by eye, the intersection defining the corner frequency (f_c) indicated by the arrow. The seismograms selected are from the microearthquake of 1983 January 6 of magnitude 2.8 M_L recorded at (a) station PT1 (Patras University), hypocentral distance 7.0 km, and (b) station PT3b (Araxos), hypocentral distance 38.9 km.

over a circular fault area, is given by

$$s = M_0/\mu\pi r^2 \quad \text{(in m)} \tag{4}$$

(Brune 1968), where μ is the shear modulus (typically 3×10^{10} N m^{-2}). Seismic moments and fault radii are determined by averaging the values calculated for each station. As measurements of both seismic moment and fault radius are log-normally distributed, the best estimates are the geometric means (Archuleta *et al.* 1982). Rather than giving a standard deviation on these estimates, maximum and

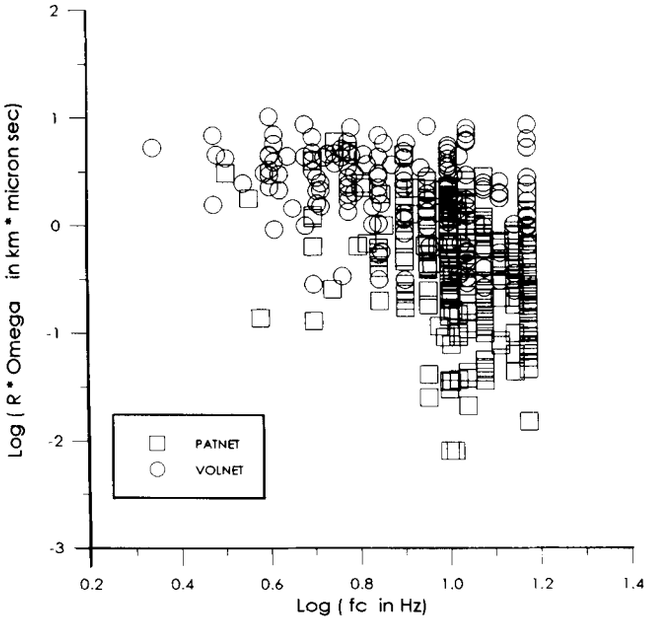

Figure 8. The family of Ω_0 and f_c values obtained from all the spectra analysed (see Fig. 7), with $R\Omega_0$ values compensating for hypocentral distance R km.

minimum values are calculated to show the overall range within which the parameters lie. A similar procedure is followed to determine stress drop and average slip (Gagnepain-Beyneix 1985), again including minimum and maximum values as well as the best estimate of each parameter. Results for seismic moment, fault radius, stress drop and coseismic slip were obtained for 94 of the 108 events. Fig. 9 shows the epicentral distribution of these 94 events and Table 4 lists the corresponding results.

The source parameters for these microearthquakes, within the local magnitude range 1.8 to 3.9 M_L, are in the following ranges: (a) seismic moment, M_0: 0.3 to 45.7×10^{12} Nm; (b) source radius, r: 72 to 310 m; (c) stress drop, $\Delta\sigma$: 0.7 to 174.6 bar; and (d) average seismic slip: 0.36 to 41.17 mm.

The results show a wide range of stress drops (0.7 to 174.6 bar), within which stress drop, coseismic slip and seismic moment all correlate well. Correlated variations in fault radius are almost imperceptible for the whole range of seismic moments, stress drops and average coseismic slips. However, there is a distinctive set of nine events that show higher fault radii than the rest of the data set, accompanied by relatively higher seismic moments but lower stress drops and coseismic slips (Figs 10 and 11). These nine events are located in the Corinth–Trikhonis zone of extension and have epicentres identified in Fig. 9 with a star.

All 94 spectrally analysed events were used to produce relationships between (1) seismic moment and local magnitude, and (2) seismic moment and the seismotectonic source parameters, in order to investigate crustal deformation in the Patras area using all recorded events. The relationships were determined using double error regression analysis (York 1966).

3.1 Seismic moment and local magnitude [log(M_0) versus M_L]

Pairs of [log (M_0), M_L] values were examined, for the 94 microearthquakes of the whole data set (WDS) analysed. A relatively poor correlation coefficient, cc, of 0.55 was obtained for the following regression equation:

$$\log M_0 = 8.45(\pm 0.39) + 1.54(\pm 0.14)M_L \quad (\text{WDS}, cc = 0.55). \tag{5}$$

At first sight, it is surprising to find a relatively poor correlation between these two parameters for the Patras area and surrounding region, given the care taken to ensure that the spectral parameters (Ω_0, f_c) were measured

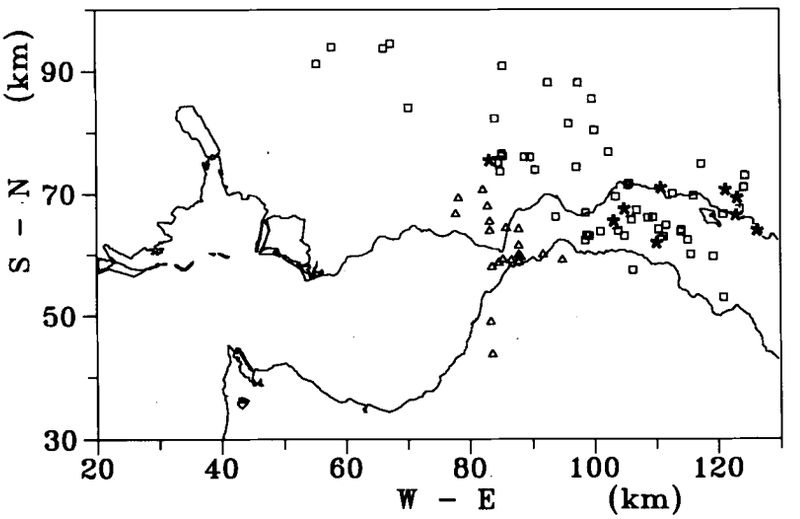

Figure 9. Distribution of the 94 epicentres for which seismotectonic source parameters were determined. Epicentres of zone 1 (Corinth–Trikhonis extension) are indicated with box symbols and epicentres of zone 2 (Rio graben transtension) with triangles. The stars indicate the nine microearthquakes that show relatively higher values of seismic moment and source radius, but lower values of stress drop and average coseismic slip.

Table 4. Seismotectonic source parameters for 94 of the well-located microearthquakes in the Patras area. M_L = local magnitude given by PATNET or VOLNET, M_0 = seismic moment ($\times 10^{12}$ N m), r = fault radius (m), $\Delta\sigma$ = stress drop (bar), s = slip (mm), No = number of Ω_0 readings, and Nf = Number of f_c readings. The values above and below each calculated parameter are the maximum and minimum, respectively, indicating the range within which the value is defined.

No Event	M_L	Mo ($\times 10^{12}$ Nm)	r (m)	$\Delta\sigma$ (bars)	s (mm)	No (Ω_0)	Nf (f_c)
PATNET located events							
1	2.8	25.7 10.9 4.7	129.3 104.7 84.8	117.3 41.7 14.8	20.12 10.59 5.57	6	6
2	2.9	9.5 5.2 2.9	97.9 78.4 62.8	143.8 47.5 15.7	18.11 9.03 4.50	5	4
3	2.3	5.7 2.4 1.0	93.3 76.1 62.1	73.9 24.0 7.8	9.22 4.44 2.13	5	5
4	3.1	15.2 6.7 2.9	116.4 91.2 71.4	130.3 38.5 11.4	18.25 8.50 3.96	5	4
5	1.8	1.7 0.8 0.3	79.2 72.1 65.6	17.1 8.8 4.5	2.46 1.53 0.95	5	2
6	3.2	2.0 1.5 1.1	267.1 207.5 161.2	2.8 0.7 0.2	0.85 0.36 0.15	4	4
7	2.6	1.7 0.6 0.2	112.9 92.9 76.5	12.0 3.5 1.0	1.81 0.79 0.35	5	5
9	2.5	15.1 7.3 3.6	142.8 110.4 85.3	84.8 23.9 6.7	13.99 6.39 2.92	5	5
11	2.2	2.6 1.1 0.5	94.2 80.4 68.7	24.8 9.5 3.7	3.53 1.86 0.98	3	2
12	2.5	13.8 7.4 3.9	109.9 103.4 97.2	43.4 29.1 19.5	9.57 7.30 5.57	5	4
13	2.6	1.3 0.6 0.2	119.3 95.0 75.6	11.6 2.9 0.7	1.68 0.67 0.27	5	5
14	2.4	2.0 1.3 0.8	116.8 95.5 78.0	19.6 6.4 2.1	3.04 1.48 0.72	5	5
15	3.0	9.8 5.3 2.8	119.9 119.9 119.9	17.9 13.4 10.1	4.84 3.90 3.15	2	2
17	2.2	3.1 2.1 1.4	98.4 84.6 72.8	33.6 14.9 6.6	5.15 3.06 1.81	5	3
19	2.2	3.5 1.5 0.6	91.4 86.4 81.6	17.0 10.1 6.0	3.10 2.12 1.45	5	2
20	3.1	12.2 6.3 3.3	159.3 127.0 101.3	42.1 13.5 4.4	8.43 4.17 2.07	6	6
21	2.8	18.7 10.0 5.3	250.4 162.4 105.3	79.5 10.2 1.3	13.83 4.02 1.17	5	5
22	2.7	9.4 7.0 5.3	134.1 125.6 117.6	21.9 15.5 11.0	5.87 4.73 3.82	5	2
23	2.6	3.0 1.9 1.1	121.0 95.2 74.9	34.1 9.4 2.6	4.94 2.17 0.96	5	5
24	2.6	2.3 1.1 0.5	130.1 103.6 82.6	15.8 4.3 1.2	2.52 1.08 0.46	5	5
25	2.6	9.3 5.1 2.8	162.8 117.9 85.4	68.2 13.7 2.7	10.57 3.92 1.45	5	5
26	3.5	10.7 8.7 7.1	254.1 145.5 83.3	173.6 12.4 0.9	21.47 4.38 0.89	2	2

Table 4. (*Continued.*)

No Event	M_L	Mo ($\times 10^{12}$ Nm)	r (m)	$\Delta\sigma$ (bars)	s (mm)	No (Ω_0)	Nf (f_c)
27	2.3	2.3 0.9 0.4	106.4 87.6 72.1	19.3 5.9 1.8	2.77 1.26 0.58	5	4
28	2.5	16.0 6.4 2.6	118.7 89.0 66.8	166.5 39.7 9.5	21.03 8.57 3.50	5	4
29	2.3	2.3 1.6 1.1	124.8 100.8 81.5	21.1 6.7 2.1	3.40 1.63 .78	4	4
30	2.7	22.1 14.1 9.0	113.5 102.2 92.1	95.7 57.8 34.9	19.56 14.32 10.49	5	5
32	2.4	12.7 3.7 1.1	103.5 78.9 60.1	141.1 32.7 7.6	16.10 6.25 2.43	5	3
33	3.1	12.5 3.6 1.0	123.0 99.8 81.0	52.3 15.7 4.7	8.38 3.81 1.73	5	5
34	3.9	109.0 44.4 18.1	396.5 310.2 242.7	20.2 6.5 2.1	9.51 4.90 2.52	5	5
35	2.6	7.3 2.7 1.0	105.5 82.5 64.5	79.9 20.8 5.4	9.96 4.17 1.75	5	5
36	2.6	18.1 14.5 11.5	115.5 110.2 105.1	59.6 47.3 37.5	14.58 12.63 10.94	5	5
37	2.2	3.2 1.4 0.7	107.5 101.9 96.6	9.7 5.9 3.6	2.11 1.47 1.02	4	2
38	2.2	4.3 1.9 0.8	101.5 90.2 80.2	23.5 11.2 5.4	4.05 2.46 1.50	4	2
39	3.1	5.2 4.1 3.3	140.6 115.2 94.4	32.2 11.9 4.4	6.14 3.31 1.78	5	4
40	2.4	5.7 3.6 2.3	79.6 73.7 68.2	60.6 39.2 25.4	9.34 7.01 5.26	5	3

Table 4. (*Continued.*)

No Event	M_L	Mo ($\times 10^{12}$ Nm)	r (m)	$\Delta\sigma$ (bars)	s (mm)	No (Ω_0)	Nf (f_c)
41	2.3	4.1 1.9 0.9	77.0 72.0 67.4	36.2 21.9 13.2	5.48 3.82 2.67	5	3
42	2.7	24.5 9.8 3.9	136.2 96.3 68.0	250.7 47.9 9.1	30.91 11.18 4.04	5	3
43	2.8	8.5 5.4 3.4	88.7 81.1 74.2	71.1 44.3 27.6	11.82 8.71 6.42	5	3
45	2.9	1.3 0.3 0.1	118.9 94.8 75.5	8.1 1.7 0.4	1.15 0.39 0.13	5	4
46	2.1	14.6 8.6 5.1	135.3 104.5 80.6	114.2 33.1 9.6	17.90 8.39 3.93	5	5
47	2.8	19.0 7.2 2.7	172.9 131.4 100.0	55.4 13.9 3.5	10.46 4.42 1.87	5	5
48	2.4	11.4 6.6 3.9	102.7 82.8 66.8	146.2 51.1 17.8	19.74 10.26 5.33	4	4
49	2.5	3.5 2.8 2.2	110.9 87.8 69.5	59.9 18.0 5.4	8.16 3.84 1.80	4	4
50	2.3	2.6 1.5 0.9	104.5 87.3 72.9	27.1 9.9 3.6	4.02 2.10 1.10	5	3
51	2.9	22.4 9.8 4.3	141.5 114.5 92.7	81.8 28.7 10.1	15.26 7.96 4.16	5	5
52	2.1	0.6 0.4 0.3	102.3 99.6 97.0	2.4 1.8 1.3	0.55 0.44 0.35	5	3
53	2.5	5.0 2.5 1.2	115.4 85.4 63.2	84.8 17.3 3.5	9.86 3.58 1.30	5	3
54	2.8	12.4 5.1 2.1	108.3 98.0 88.7	44.3 23.7 12.6	8.59 5.62 3.68	5	4

Table 4. (*Continued.*)

No Event	M_L	Mo ($\times 10^{12}$ Nm)	r (m)	Δσ (bars)	s (mm)	No (Ω_o)	Nf (f_c)
55	2.9	16.6 8.6 4.5	147.2 107.1 77.8	141.3 30.8 6.7	20.31 7.99 3.14	5	5
56	2.8	7.7 2.4 0.7	119.4 101.0 85.4	28.6 10.1 3.6	4.98 2.48 1.23	5	5
57	2.7	12.1 6.1 3.0	121.0 100.3 83.2	68.3 26.3 10.1	11.66 6.40 3.51	5	5
58	2.6	3.5 1.2 0.4	119.7 113.4 107.5	6.8 3.5 1.8	1.59 0.97 0.59	5	4
59	2.8	11.9 7.1 4.3	140.1 98.6 69.3	177.0 32.6 6.0	22.02 7.80 2.76	5	5
60	2.0	4.7 1.2 0.3	91.0 81.3 72.6	24.5 9.8 3.9	3.75 1.94 1.00	5	3
61	2.9	4.5 2.6 1.5	109.6 89.5 73.1	46.8 16.0 5.5	6.88 3.48 1.76	5	4
62	2.6	13.4 4.5 1.5	109.9 88.7 71.6	89.8 28.1 8.8	12.81 6.05 2.86	5	4
63	3.1	2.0 0.6 0.2	104.9 96.2 88.2	6.6 2.7 1.1	1.23 0.64 0.33	5	4
64	2.8	14.7 9.3 5.8	114.5 95.8 80.1	108.5 46.2 19.6	18.13 10.72 6.34	5	5
65	2.8	6.0 3.5 2.1	136.0 110.9 90.4	32.7 11.3 3.9	5.93 3.05 1.57	5	5
66	2.8	4.4 1.5 0.5	117.8 97.6 80.8	22.0 6.9 2.2	3.56 1.64 0.76	5	5
67	2.4	7.5 4.7 2.9	106.6 96.9 88.1	37.8 22.6 13.5	7.39 5.30 3.81	5	3

Table 4. (*Continued.*)

No Event	M_L	Mo ($\times 10^{12}$ Nm)	r (m)	Δσ (bars)	s (mm)	No (Ω_o)	Nf (f_c)
68	2.3	5.4 1.2 0.3	118.9 85.3 61.2	60.4 8.5 1.2	6.45 1.76 0.48	5	2
69	2.8	19.2 8.5 3.8	103.5 83.6 67.5	183.0 64.0 22.4	25.04 12.97 6.72	5	4
70	2.4	3.1 2.3 1.7	112.1 98.5 86.6	20.8 10.5 5.3	3.88 2.51 1.63	5	2
VOLNET located events							
1	2.5	4.7 3.5 2.7	102.6 99.9 97.3	18.6 15.5 12.9	4.27 3.76 3.31	5	2
3	3.2	40.6 21.0 10.9	303.2 180.7 107.7	159.1 15.6 1.5	26.75 6.82 1.74	8	8
4	2.9	14.7 11.5 9.0	91.3 77.6 66.0	226.8 107.5 51.0	31.89 20.24 12.84	7	6
5	2.8	34.7 21.4 13.2	244.0 217.1 193.1	16.1 9.1 5.2	6.79 4.81 3.41	7	7
6	2.8	5.9 3.5 2.0	184.1 105.5 60.5	216.6 13.0 0.8	19.14 3.32 0.57	8	6
7	3.3	36.7 18.3 9.1	304.7 189.7 118.1	101.5 11.7 1.3	19.28 5.38 1.50	7	7
10	2.8	16.9 10.0 5.9	122.4 84.6 58.5	401.6 72.2 13.0	42.23 14.81 5.20	8	7
11	3.3	13.0 8.1 5.0	97.4 73.6 55.6	334.4 88.7 23.5	35.91 15.83 6.98	8	6
12	3.0	46.0 28.8 18.0	242.4 184.9 141.1	65.7 19.9 6.0	17.93 8.92 4.44	8	8

Table 4. (*Continued.*)

No Event	M_L	Mo ($\times 10^{12}$ Nm)	r (m)	$\Delta\sigma$ (bars)	s (mm)	No (Ω_0)	Nf (f_c)
13	2.9	22.0 12.5 7.1	163.6 123.7 93.6	106.0 28.8 7.8	18.97 8.63 3.93	8	8
14	3.4	18.6 9.2 4.5	217.1 181.6 151.9	16.6 6.7 2.7	5.18 2.95 1.68	7	7
15	3.0	14.5 8.1 4.6	172.2 107.3 66.8	273.1 28.8 3.0	29.53 7.49 1.90	7	7
16	3.0	12.0 9.8 8.0	138.9 125.8 113.8	34.6 21.6 13.4	8.77 6.58 4.93	5	5
17	3.0	3.7 3.0 2.4	126.1 86.4 59.2	141.0 20.5 3.0	14.40 4.30 1.28	5	5
18	2.8	17.7 13.4 10.2	230.6 163.2 115.5	66.4 13.5 2.7	13.79 5.34 2.07	7	7
19	3.0	26.4 17.4 11.4	189.0 145.7 112.3	80.1 24.6 7.5	17.52 8.68 4.30	7	6
20	2.6	9.3 6.6 4.6	148.3 115.1 89.3	64.4 18.9 5.5	11.17 5.26 2.48	7	3
21	2.9	72.6 45.7 28.8	136.1 108.5 86.6	399.8 156.4 61.2	70.93 41.17 23.90	8	7
22	2.7	9.6 4.9 2.5	141.3 120.6 103.0	28.4 12.3 5.3	6.12 3.60 2.12	4	2
23	2.5	3.3 2.5 1.9	220.3 148.3 99.9	25.8 3.3 0.4	4.28 1.20 0.34	6	3
25	2.4	5.3 3.8 2.7	101.5 90.2 80.2	42.0 22.8 12.4	7.34 5.00 3.40	6	2
27	3.2	20.3 11.2 6.1	111.1 93.4 78.6	137.4 59.9 26.1	22.65 13.56 8.12	8	3
28	2.9	6.8 4.4 2.9	53.1 48.1 43.6	289.4 174.6 105.3	28.28 20.37 14.68	6	4
30	2.8	2.7 1.8 1.3	60.9 56.5 52.5	68.5 44.8 29.3	8.15 6.14 4.63	8	4
32	3.2	6.8 5.3 4.2	100.9 72.4 51.9	310.3 61.6 12.2	29.58 10.82 3.96	6	5
33	2.7	11.7 5.2 2.3	84.3 80.0 75.9	67.9 44.2 28.8	11.65 8.58 6.32	4	2
34	2.6	4.3 2.9 1.9	99.9 93.9 88.3	21.9 15.2 10.6	4.42 3.47 2.72	5	2
35	3.0	57.6 40.6 28.6	148.7 121.7 99.5	229.4 98.5 42.3	47.46 29.07 17.81	9	7
36	2.9	8.9 6.0 4.0	224.7 186.1 154.1	10.4 4.1 1.6	3.27 1.84 1.03	7	3
38	3.0	10.0 6.9 4.8	113.1 102.9 93.5	45.1 27.9 17.3	9.41 6.97 5.15	8	4

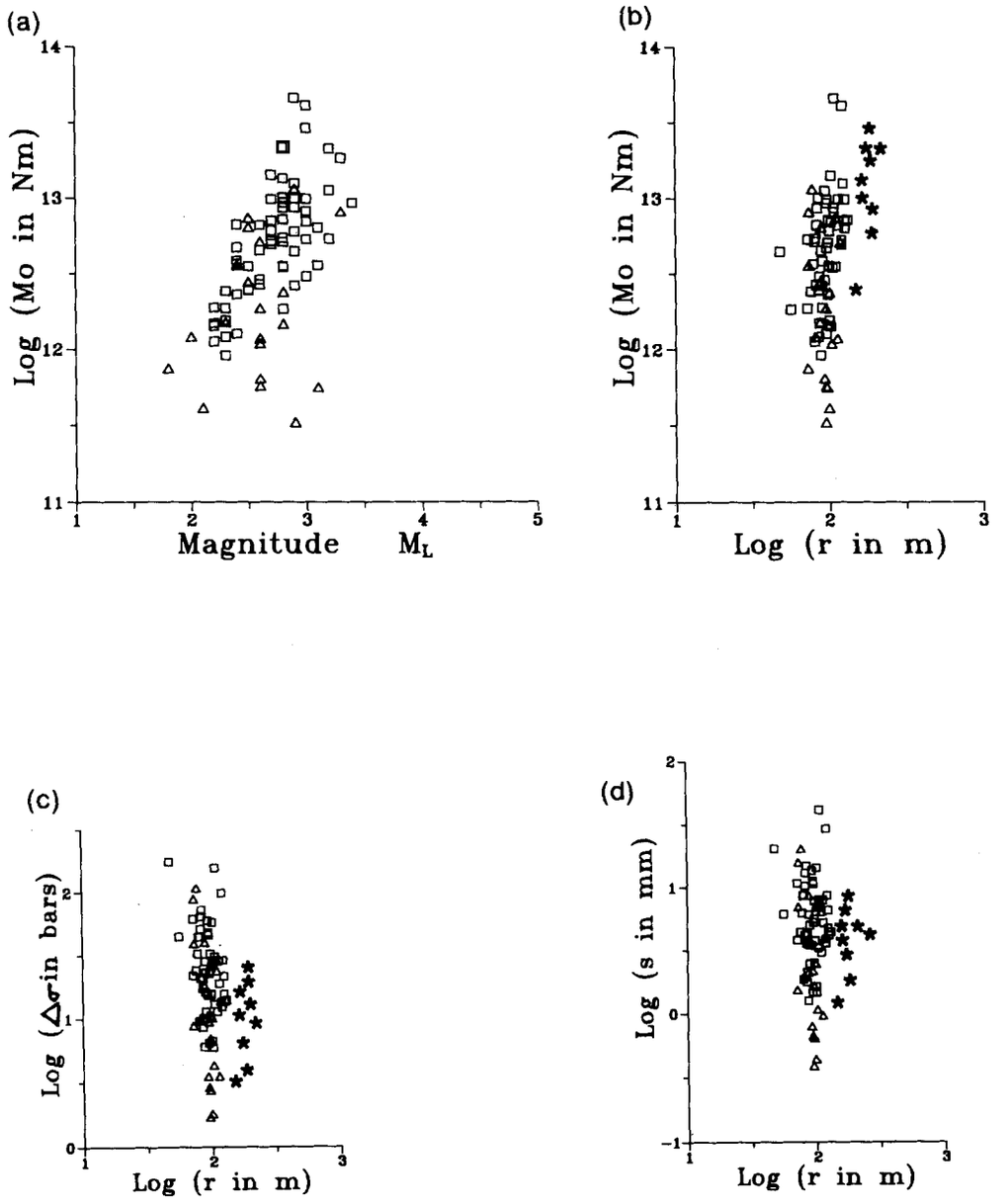

Figure 10. Seismic moment, local magnitude and seismotectonic fault radius for the Patras area. (a) Log (M_0) versus M_L and (b)–(d) show, respectively, log (M_0), log ($\Delta\sigma$) and log (s) versus log (r). Zone 1 (Corinth–Trikhonis extension)—box symbols; zone 2 (Rio graben transtension)—triangles; anomalous events (see Fig. 9)—star symbols.

accurately. However, bearing in mind the complexity of the neotectonic regime in the area (Brooks *et al.* 1988; Melis *et al.* 1989), it was decided to investigate the correlations in two internal zones of differing neotectonic setting. Zone 1 (z1) covers the Corinth–Trikhonis extensional regime and contains 62 events. Zone 2 (z2) covers the Rio graben transtensional regime and contains 20 events. Fig. 9 shows the overall distribution of epicentres and the internal subdivision into these two zones. Thus, these two subsets are used to study the correlations in smaller structural zones than is possible using the full 94 event data set. Pairs of [log (M_0), M_L] values are plotted in Fig. 10(a) for both zone 1 and zone 2 data subsets. The following equations are obtained from double error regression between the parameters for each of the two data subsets:

$$\log M_0 = 8.85(\pm 0.38) + 1.42(\pm 0.14)M_L \quad (z1, cc = 0.69), \quad (6)$$

and

$$\log M_0 = 5.8(\pm 1.5) + 2.49(\pm 0.56)M_L \quad (z2, cc = 0.25). \quad (7)$$

The correlation coefficient improves for the zone 1 subset but is worse for zone 2. Attempting to improve the correlation for zone 1 by omitting the nine anomalous events produces

$$\log M_0 = 8.85(\pm 0.42) + 1.42(\pm 0.15)M_L \quad (z1', cc = 0.67), \quad (8)$$

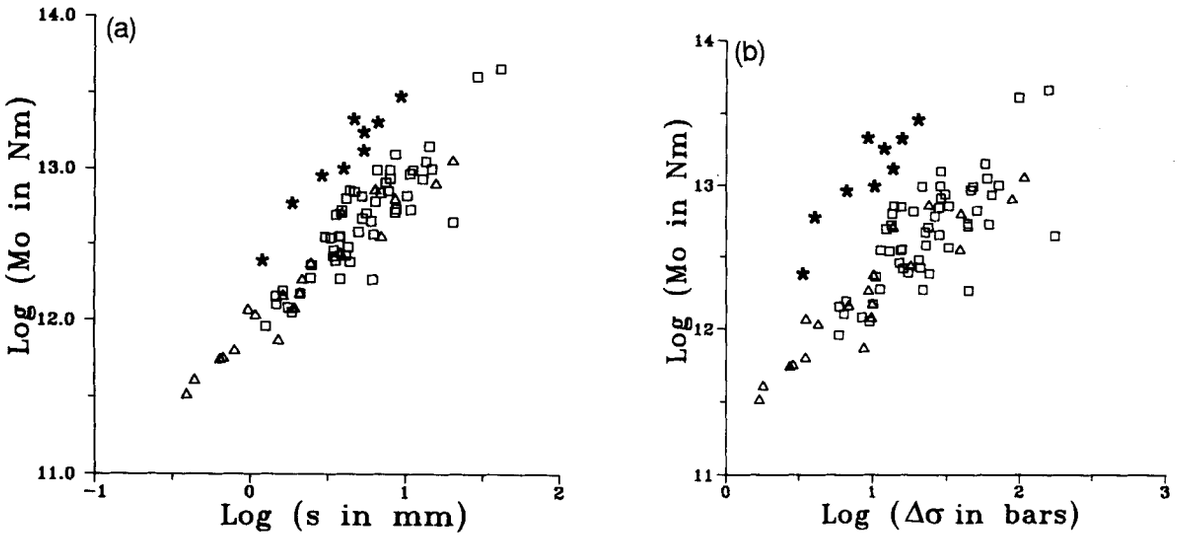

Figure 11. Seismic moment, average coseismic slip and stress drop for the Patras area. (a) Log (M_0) versus s, and (b) Log (M_0) versus $\Delta\sigma$. Zone 1 (Corinth–Trikhonis extension)—box symbols; zone 2 (Rio graben transtension)—triangles; anomalous events (see Fig. 9)—star symbols.

with a correlation coefficient of 0.67, thus making no significant difference.

Clearly, an accurate calculation of seismic moment M_0 for events with known local magnitude M_L cannot be made for these zones in the Patras area, thus precluding from the detailed investigation those events for which spectral analysis has not been explicitly carried out. The correlations of seismic moment with other calculated seismotectonic source parameters can be obtained, as below, and used for further investigation of these source characteristics in the smaller zones identified in the Patras area.

3.2 Seismic moment and fault radius [log (M_0) versus log (r)]

Pairs of [log (M_0), log (r)] values analysed for the whole data set and zone 1 and zone 2 subsets (Fig. 10b) result in

$$\log M_0 = -2.0(\pm 1.4) + 7.28(\pm 0.67) \log r \quad \text{(WDS, } cc = 0.46\text{)}, \tag{9}$$

$$\log M_0 = 2.5(\pm 1.1) + 5.07(\pm 0.54) \log r \quad \text{(z1, } cc = 0.55\text{)} \tag{10}$$

and

$$\log M_0 = 98.(\pm 20.) - 43.9(\pm 9.7) \log r \quad \text{(z2, } cc = -0.17\text{)}. \tag{11}$$

All three cases produce a poor correlation coefficient, although a slight improvement is apparent for zone 1 in comparison with the whole data set. Zone 1, omitting the nine anomalous events, produces

$$\log M_0 = -6.4(\pm 2.4) + 9.6(\pm 1.2) \log r \quad \text{(z1', } cc = 0.42\text{)}. \tag{12}$$

The correlation between seismic moment and source radius is very poor and precludes its further use. The source radius is effectively constant, within its range of uncertainty, for a wide range of seismic moments, stress drops and average coseismic slips (see Fig. 10b).

3.3 Seismic moment and slip [log (M_0) versus log s]

Analysis of pairs of [log (M_0), log (s)] values produces (Fig. 11a)

$$\log M_0 = 11.9(\pm 0.1) + 1.14(\pm 0.07) \log s \quad \text{(WDS, } cc = 0.83\text{)}, \tag{13}$$

$$\log M_0 = 11.8(\pm 0.1) + 1.26(\pm 0.11) \log s \quad \text{(z1, } cc = 0.75\text{)} \tag{14}$$

and

$$\log M_0 = 11.93(\pm 0.03) + 0.93(\pm 0.05) \log s \quad \text{(z2, } cc = 0.97\text{)}. \tag{15}$$

There is a small deterioration of the correlation coefficient for the zone 1 subset and this is discussed in Section 4 below. Omitting the nine anomalous events from the whole data set gives

$$\log M_0 = 11.91(\pm 0.04) + 1.06(\pm 0.06) \log s \quad \text{(WDS', } cc = 0.89\text{)}, \tag{16}$$

and, from zone 1,

$$\log M_0 = 11.8(\pm 0.1) + 1.11(\pm 0.07) \log s \quad \text{(z1', } cc = 0.89\text{)}, \tag{17}$$

while the nine events by themselves produce

$$\log M_0 = 12.4(\pm 0.1) + 1.20(\pm 0.10) \log s \quad (cc = 0.97). \tag{18}$$

We conclude that the correlation between seismic moment and average coseismic slip is generally excellent. However, poor correlation of seismic moment with local magnitude unfortunately prevents extension to the other micro-earthquakes recorded in the Patras area.

3.4 Seismic moment and stress drop [log (M_0) versus log ($\Delta\sigma$)]

Analysis of [log (M_0), log ($\Delta\sigma$)] pairs produces (Fig. 11b)

$$\log M_0 = 11.3(\pm 0.1) + 1.05(\pm 0.09) \log \Delta\sigma \quad (\mathrm{WDS}, cc = 0.63), \tag{19}$$

$$\log M_0 = 11.2(\pm 0.2) + 1.12(\pm 0.14) \log \Delta\sigma \quad (\mathrm{z1}, cc = 0.48) \tag{20}$$

and

$$\log M_0 = 11.4(\pm 0.1) + 0.87(\pm 0.07) \log \Delta\sigma \quad (\mathrm{z2}, cc = 0.94). \tag{21}$$

Equation (19) shows reasonable correlation, but, again, this deteriorates for the zone 1 subset, because the well-correlated data of zone 2 are omitted and zone 1 contains nine events with an anomalous and distinctive character (see Figs 9 and 11b). Omitting the nine anomalous events from zone 1 produces

$$\log M_0 = 11.2(\pm 0.2) + 1.07(\pm 0.11) \log \Delta\sigma \quad (\mathrm{z1}', cc = 0.74), \tag{22}$$

and omitting the same nine events from the whole data set now gives

$$\log M_0 = 11.3(\pm 0.1) + 0.99(\pm 0.08) \log \Delta\sigma \quad (\mathrm{WDS}', cc = 0.75), \tag{23}$$

resulting in an impressive improvement for all subsets. The nine anomalous events by themselves produce

$$\log M_0 = 11.8(\pm 0.2) + 1.30(\pm 0.18) \log \Delta\sigma \qquad (cc = 0.91). \tag{24}$$

First, we conclude that correlation between seismic moment and stress drop is generally good in the cases examined here (and generally excellent between moment and average coseismic slip). Nevertheless, the poor correlation with local magnitude (6) still prevails, rendering extension to non-spectrally analysed events in the zone tenuous with the data sets available to us. Secondly, we conclude that scaling between seismic moment and stress drop in the Patras area exists even for events with low seismic moment. This result is in agreement with other studies (e.g. Aki 1967; Archuleta 1986; van Eck & Hofstetter 1989; Burton *et al.* 1995).

In summary, the whole data set of 94 spectrally analysed microearthquakes does not provide a good correlation between local magnitude and seismic moment either overall or in smaller subsets. Also, the correlation is often poor between seismic moment and the seismotectonic source parameters, although it is improved by careful choice of specific subsets of data. The likely reason is the complex nature of the neotectonic regime existing in the area (Brooks *et al.* 1988; Melis *et al.* 1989). The analysis also suggests that zone 1 (Corinth–Trikhonis) has two sets of characteristic faults. The first set is represented by nine events, showing distinctive and unusual relatively high seismic moments existing with low stress drops and seismic slips. This set of faults shows greater source radius than the second set and therefore these faults are longer. The second set is characterized by almost constant source radius, a wide range of seismic moments, stress drops and seismic slips, similar to other studies (see previous paragraph).

Examination of the anomalous events in the first fault set shows that eight of the nine are recorded by the Volos network and only one by the Patras network. This might suggest that the correction for attenuation has affected the measured spectral parameters (Ω_0 and f_c) and, hence, the source parameters. Checking this possibility shows that it can be discounted because the effect of the Q-correction can be seen to be insignificant for the measured spectral parameters. Moreover, the anomalous event recorded by the Patras network indicates no changes with or without a Q-correction. Thus, it is concluded that all nine events are consistently anomalous with respect to both the whole data set and the zone 1 subset.

4 COSEISMIC CRUSTAL DEFORMATION IN THE PATRAS AREA

As shown above, a good correlation between local magnitude and seismic moment could not be obtained from the 94 spectrally analysed events for the Patras area, and this precludes extension to the full data sets of VOLNET and PATNET microearthquakes. However, the 94 event data set is in itself a sufficiently large sample to investigate crustal deformation in the Patras area.

The study area is divided into 2.5 km × 2.5 km cells and, first, the sum of seismic slips is calculated for each cell. The geometric mean of coseismic slip is contoured using all 94 events. A window is then defined encapsulating the Patras area (Fig. 12a). The area of the Rio–Antirrio crossing is characterized by low seismic slip, whereas the city of Patras, the west end of the Gulf of Corinth and the area between Trikhonis Lake and Nafpaktos exhibit relatively higher values of seismic slip. There is a concentration of low-slip events at the Rio–Antirrio crossing.

In a similar way, the geometric means of stress drop and source radius are calculated for each predefined cell and then contoured. The window enclosing the Patras area is shown for these two source parameters in Figs 12(b) and (c). Low stress drop is apparent at the Rio–Antirrio crossing, whereas at the city of Patras, the Gulf of Corinth and the area between Trikhonis Lake and Nafpaktos, higher stress drop is observed. Finally, for the source radius, relatively high values are shown at the east end of the Narrows, south-east of Trikhonis and south-east of the Gulf of Patras. Lower values are shown for the rest of the region, with a minimum occurring in the Gulf of Corinth near Egio.

5 CONCLUSIONS

A set of well-located microearthquakes in the Patras area and its surrounding region was selected for spectral analysis, to determine seismotectonic source parameters using a procedure described elsewhere (Melis 1992; Burton *et al.* 1995). The results show poor correlation between seismic moment and local magnitude, but in some cases good correlation exists between seismic moment and some of the

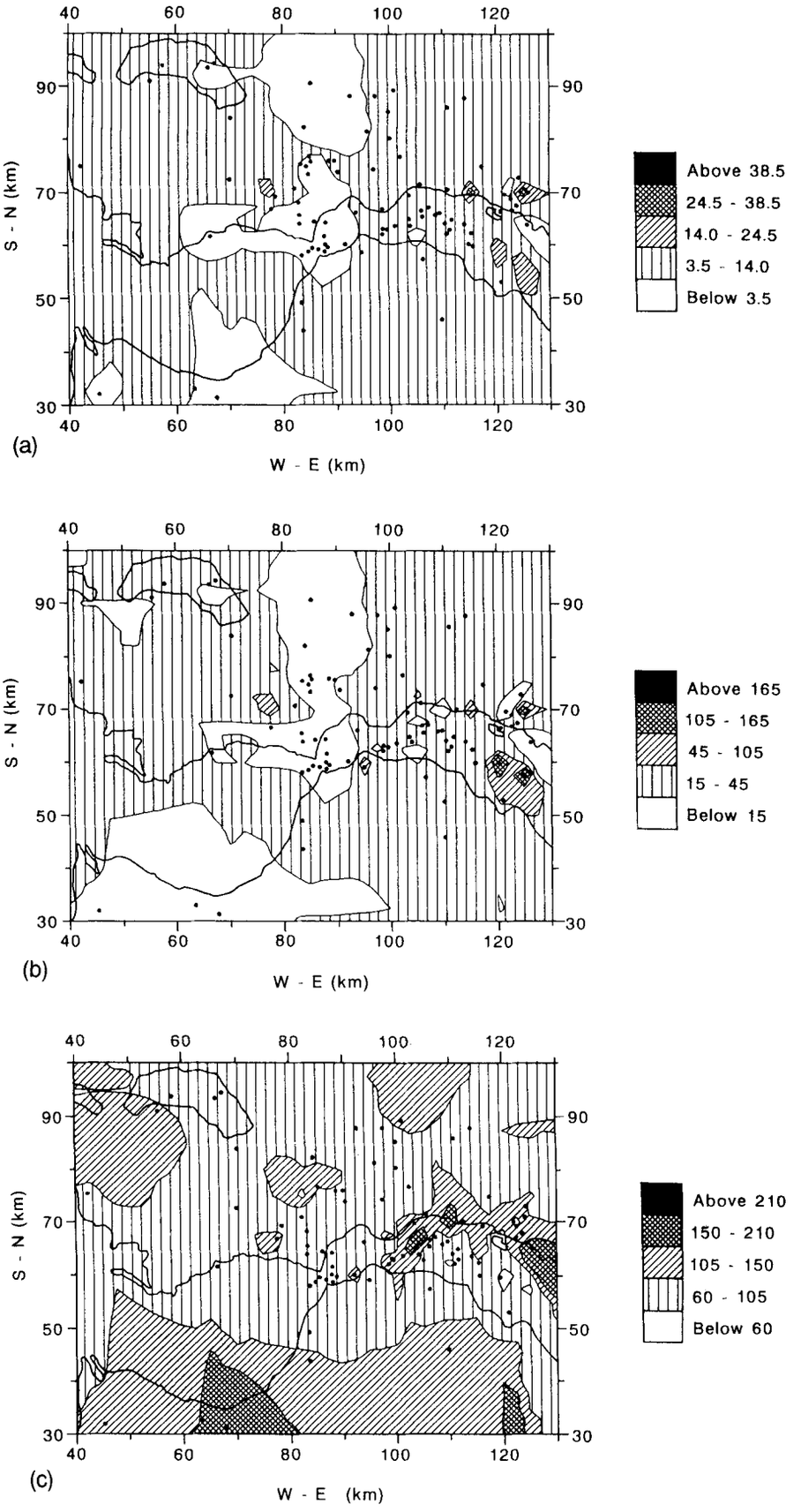

Figure 12. (a) Geometric mean of coseismic slip (mm) contoured in the Patras area. (b) Geometric mean of stress drop (bar) contoured in the Patras area. (c) Geometric mean of source radius (m) contoured in the Patras area.

calculated seismotectonic source parameters, particularly when they are carefully zoned.

The poor moment–magnitude correlation meant that only the 94 spectrally analysed microearthquakes could be used, and precluded any extension through the correlation equation to the full data set of microearthquakes recorded in the area. However, the former data set is a large statistical sample of the earthquakes recorded. Hence, contouring of geometric mean values of source parameters was performed for a predefined 2.5 km ×2.5 km grid, and a window encapsulating the Patras area was used to display regional variations in the seismic slip, stress drop and source radius.

The Rio–Antirrio district is characterized by a high activity of events of low source radius, stress drop and seismic slip, whereas the city of Patras is shown to encounter low source radius, relatively high stress drop and medium seismic slip events. This contrasts with the Gulf of Corinth, which has higher stress drop, medium to high seismic slip and relatively low source radius events. Finally, the Trikhonis–Nafpaktos area reveals a higher stress drop, accompanied by low seismic slip and source radius, with the exception of one locality north of Nafpaktos, where high source radius and seismic slip are observed.

ACKNOWLEDGMENTS

The Patras seismic network was supported by the Universities of Cardiff and Patras, and the Volos seismic network by the British Geological Survey and the University of Athens, including support from the Natural Environment Research Council and assistance with data transmission from the British Embassy. The data in Table 3 were kindly given to us by Denis Hatzfeld. NSM thanks the University of Wales for a scholarship, and Dr R. Fantechi at the Directorate General for Science, Research and Development of the European Communities for generous financial support (EC Sectoral Grant B/86000071). This work was also supported in part by NERC Grant GR9/1005.

REFERENCES

Aki, K., 1967. Scaling law of seismic spectrum, *J. geophys. Res.*, **84,** 6140–6148.

Ambraseys, N.N. & Jackson, J.A., 1990. Seismicity and associated strain of central Greece between 1890 and 1988, *Geophys. J. Int.*, **101,** 663–708.

Archuleta, R.J., 1986. Downhole recordings of seismic radiation, in *Earthquake Source Mechanics, Am. geophys. Un. Monogr.*, **37,** 319–329.

Archuleta, R.J., Granswick, E., Mueller, C. & Spudich, P., 1982. Source parameters of the 1980 Mammoth Lakes, California, earthquake sequence, *J. geophys. Res.*, **87,** 4595–4607.

Brooks, M. & Ferentinos, G., 1984. Tectonics and sedimentation in the Gulf of Corinth and the Zakynthos and Kefallinia Channels, western Greece, *Tectonophysics*, **101,** 25–54.

Brooks, M., Clews, J.E., Melis, N.S. & Underhill, J.R., 1988. Structural development of Neogene basins in western Greece, *Basin Res.*, **1,** 129–138.

Brune, J.N., 1968, Seismic moment, seismicity, and rate of slip along major fault zones, *J. geophys. Res.*, **73,** 777–784.

Brune, J.N., 1970. Tectonic stress and the spectra of seismic shear waves from earthquakes, *J. geophys. Res.*, **75,** 4997–5009.

Brune, J.N., 1971. Correction. *J. geophys. Res.*, **76,** 5002.

Brune, J.N., Fletcher, J.B., Vernon, F.L., Haar, L., Hanks, T.C. & Berger, J., 1986. Low stress-drop earthquakes in the light of new data from the Anza, California telemetered digital array, in *Earthquake Source Mechanics, Am. geophys. Un. Monogr.*, **37,** 237–245.

Burton, P.W. & Marrow, C., 1989. Seismic hazard and earthquake source parameters in the North Sea, in *Earthquakes at North-Atlantic Passive Margins: Neotectonics and Postglacial rebound*, NATO Series C: Mathematical and Physical Sciences, Vol. 266, pp. 633–664, Kluwer Academic Publishers, Dordrecht.

Burton, P.W., Makropoulos, K.C., McGonigle, R.W., Ritchie, M.E.A., Main, I.G., Kouskouna, V. & Drakopoulos, J., 1991. Contemporary seismicity on the Nea Ankhialos fault, eastern Greece: fault parameters of major and minor earthquakes, Technical Report, WL/91/29, *Seismology Series*, BGS, Edinburgh.

Burton, P.W., McGonigle, R.W., Ritchie, M.E.A., Raines, M.G., Morgan, S.N., Makropoulos, K.C. & Agelis, S., 1983–84. VOLNET Station Bulletins, Jan. 1983–Dec. 1984, Brit. Geol. Survey & University of Athens, Joint open file reports.

Burton, P.W., Melis, N. S. & Brooks, M., 1995. Coseismic crustal deformation on a fault zone defined by microseismicity in the Pavliani area, Central Greece, *Geophys. J. Int.*, **123,** 16–40.

Chronis, G., Piper, D.J.W. & Anagnostou, C., 1991. Late Quaternary evolution of the Gulf of Patras, Greece: Tectonism, deltaic sedimentation and sea-level change, *Mar. Geol.*, **97,** 181–209.

Chronis, G., Alexandri, M., Konstantinidou, R., Chatziagelakis, A., Karageorgis, A., Roussakis, G., Kapsimilis, V., Barbatses, E., Chronis K. & Renieris, P., 1987. *Marine geological and geophysical study in Rio–Antirrio*, Internal report, National Centre of Marine Studies, Athens, Greece (in Greek).

Collier, R.E.Ll. & Dart, C.J., 1991. Neogene to Quaternary rifting, sedimentation and uplift in the Corinth Basin, Greece, *J. geol. Soc. London*, **148,** 1049–1065.

Comninakis, P.E. & Papazachos, B.C., 1986. *A catalogue of earthquakes in Greece and the surrounding area for the period* 1901–1985, Publ. Geophys. Lab., Univ. Thessaloniki, **1,** Thessaloniki.

Doutsos, T. & Piper, D.J.W., 1990. Listric faulting, sedimentation and morphological evolution of the Quaternary eastern Corinth rift, Greece: First stages of continental rifting, *Geol. Soc. Am. Bul.*, **102,** 812–829.

Doutsos, T. & Poulimenos, G., 1992. Geometry and kinematics of active faults and their seismotectonic significance in the western Corinth–Patras rift (Greece), *J. Struct. Geol.*, **14,** 689–699.

Doutsos, T., Kontopoulos, N. & Frydas, D., 1987. Neotectonic evolution of north-western continental Greece, *Geol. Rundsch.*, **76,** 433–450.

Doutsos, T., Kontopoulos, N. & Poulimenos, G., 1988. The Corinth–Patras rift as the initial stage of continental fragmentation behind an active island arc (Greece), *Basin Res.*, **1,** 177–190.

Drakopoulos, J. & Delibasis, N.D., 1982. *The focal mechanism of earthquakes in the major area of Greece for the period 1974–1981*, Publ. No. 2, Seismological Laboratory, University of Athens.

Ferentinos, G., Brooks, M. & Doutsos, T., 1985. Quaternary tectonics in the Gulf of Patras, western Greece, *J. Struct. Geol.*, **7,** 713–717.

Gagnepain-Beyneix, J., 1985. Variation of source parameters of small western Pyrenean earthquakes and their relation to main shock occurrence, *Ann. Geophys.*, **3,** 381–394.

Galanopoulos, A.G., 1960. *A catalogue of shocks with $I_0 \geq VI$ or $M \geq 5$ for the years* 1801–1958, Seismological Laboratory, University of Athens.

Galanopoulos, A.G., 1961. *A catalogue of shocks with $I_0 \geq VII$ for*

the years prior to 1800, Seismological Laboratory, University of Athens.

Galanopoulos, A.G., 1981. The damaging shocks and the earthquake potential of Greece, *Ann. geol. Hellen.*, **XXX/2,** 647–724.

Hanks, T.C. & Wyss, M., 1972. The use of body-wave spectra in the determination of seismic source parameters, *Bull. seism. Soc. Am.*, **62,** 561–589.

Hatzfeld, D., Pedotti, G., Hatzidimitriou, P., Panagiotopoulos, D., Scordilis, M., Drakopoulos, J., Makropoulos, K., Delibasis, N., Latousakis, I., Baskoutas, J. & Frogneux, M., 1989. The Hellenic subduction beneath the Peloponnesus: first results of a microearthquake study, *Earth planet Sci. Lett.*, **93,** 283–291.

Hatzfeld, D., Pedotti, G., Hatzidimitriou, P. & Makropoulos, K., 1990. The strain pattern in the western Hellenic arc deduced from a microearthquake survey, *Geophys. J. Int.*, **101,** 181–202.

Higgs, B., 1988. Syn-sedimentary structural controls on basin deformation in the Gulf of Corinth, Greece, *Basin Res.*, **1,** 155–165.

Jackson, J.A., Gagnepain, J., Houseman, G., King, G.C.P., Papadimitriou, P., Soufleris, C. & Virieus, J., 1982. Seismicity, normal faulting, and the geomorphological development of the Gulf of Corinth (Greece): the Corinth earthquakes of February & March 1981, *Earth Planet Sci. Lett.*, **57,** 377–397.

Kanamori, H. & Anderson, D.L., 1975. Theoretical bases of some empirical relations in seismology, *Bull. seism. Soc. Am.*, **65,** 1073–1095.

Keilis-Borok, V. I., 1959. On the estimation of the displacement in an earthquake source and of source dimensions, *Ann. Geofis.*, **12,** 205–214.

King, G.C.P., Ouyang, Z.X., Papadimitriou, P., Deschamps, A., Gagnepain, J., Houseman, G., Jackson, J.A., Soufleris, C. & Virieux, J., 1985. The evolution of the Gulf of Corinth (Greece): an aftershock study of the 1981 earthquakes, *Geophys. J. R. astr. Soc.*, **80,** 677–693.

Kontopoulos, N. & Doutsos, T., 1985. Sedimentology and tectonics of the Antirrion area (western Greece), *Bull. Soc. Geol. It.*, **104,** 479–489.

Madariaga, R., 1976. Dynamics of an expanding circular fault, *Bull. seism. Soc. Am.*, **66,** 636–666.

Makropoulos, K. C. & Burton, P.W., 1981. A catalogue of seismicity in Greece and adjacent areas, *Geophys. J. R. astr. Soc.*, **65,** 741–762.

Makropoulos, K.C., Drakopoulos, J.K. & Latousakis, J.B., 1989. A revised and extended earthquake catalogue for Greece since 1900, *Geophys. J. Int.*, **98,** 391–394.

Melis, N.S., 1986. Geophysical studies of the Gulf of Patras region using the Patras Seismic Network, 1983–84, *MSc thesis,* University of Wales.

Melis, N.S., 1992. Earthquake hazard and crustal deformation in central Greece, *PhD thesis,* University of Wales.

Melis, N.S., Brooks, M. & Pearce, R.G., 1989. A microearthquake study in the Gulf of Patras region, western Greece, and its seismotectonic interpretation, *Geophys. J. R. astr. Soc.*, **98,** 515–524.

Modiano, T. & Hatzfeld, D., 1982. Experimental study of the spectral content for shallow earthquakes, *Bull. seism. Soc. Am.*, **72,** 1739–1758.

Papadopoulos, G.A., Kondopoulou, D.P., Leventakis, G.-A. & Pavlides, S.B., 1986. Seismotectonics of the Aegean region, *Tectonophysics,* **124,** 67–84.

Papazachos, B.C., 1976. Seismic activity along the Saronicos-Corinth–Patras Gulfs, *Mon. Bull. seism. Inst. nat. Obs., Athens,* 1–16.

Papazachos, B.C., 1990. Seismicity of the Aegean and surrounding area, *Tectonophysics,* **178,** 287–308.

Papazachos, B.C. & Comninakis, L., 1982a. *A catalogue of historical earthquakes in Greece and surrounding area, 479 B.C.–1900 A.D.,* University of Thessaloniki, Geophys. Lab. Publ., No. 5, Thessaloniki.

Papazachos, B.C. & Comninakis, L., 1982b. *A catalogue of earthquakes in Greece and surrounding area for the period 1901–1980,* University of Thessaloniki, Geophys. Lab. Publ., No. 6, Thessaloniki.

Papazachos, B.C. & Papazachos, C., 1989. *The Earthquakes of Greece,* Ziti, Thessaloniki.

Papazachos, B.C., Kiratzi, A.A., Hatzidimitriou, P.M. & Rocca, A.C., 1984. Seismic faults in the Aegean area, *Tectonophysics,* **106,** 71–85.

Pedotti, G., Etude sismotectonique du Peloponnese et response sismique d'une vallée sédimentaire en Grèce du Nord, *Thèse,* Université Joseph Fourier, Grenoble.

Perisoratis, K., Mitropoulos, D. & Aggelopoulos, J., 1986. Marine geological studies in the Rio–Antirrio area, *IGME report,* Athens (in Greek).

Richter, C.H., 1958. *Elementary Seismology,* W.H. Freeman, San Francisco.

Thatcher, W. & Hanks, T.C., 1973. Source parameters of Southern California earthquakes, *J. geophys. Res.*, **78,** 8547–8576.

Trifunac, M.D., 1972. Stress estimates for the San Fernando, California, earthquake of February 9, 1971: Main event and thirteen aftershocks, *Bull. seism. Soc. Am.*, **62,** 721–750.

Van Eck, T. & Hofstetter, A., 1989. Microearthquake activity in the Dead Sea region, *Geophys. J. Int.*, **99,** 605–620.

Vita-Finzi, C. & King, G.C.P., 1985. The seismicity, geomorphology and structural evolution of the Corinth area of Greece, *Phil. Trans. R. Soc. Lond.*, **314,** 379–407.

York, D., 1966. Least squares fitting of a straight line, *Can. J. Phys.*,**44,** 1079–1086.

Zelilidis, A., Koukouvelas, I. & Doutsos, T., 1987. Neogene paleostress changes behind the forearc fold belt in the Patraikos Gulf area, western Greece, *N. Jb. Geol. Palaont. Mh.*, **H5,** 311–325.